学位申請論文

謝　平平

Nephanalysis of the GMS Imagery Data

By Pingping Xie

Reprinted from the Bulletin of the Disaster Prevention Research Institute,
Kyoto University
Volume 40, June, 1990

Bull. Disas. Prev. Res. Inst., Kyoto Univ., Vol. 40, Part 2, No. 347, June 1990

Nephanalysis of the GMS Imagery Data

By Pingping XIE

(Manuscript received on May 23, 1990)

Abstract

Techniques estimating cloud amount and classifying cloud type from GMS IR and/or VIS imagery data have been developed and evaluated. Cloud amount is estimated by a Two-Threshold-Method (TTM) which takes account of the partially cloud-covered pixels. Cloud type is classified by a discriminant analysis technique. Fairly good agreement is obtained between the satellite estimated and the surface observed cloud amounts. The comparison between the satellite classified and ground observed cloud types shows correctness ratios of 52.9% and 47.7% for the daytime and nighttime respectively, but the distinction between cumulus and middle clouds seems insufficient. The techniques were applied to produce the time series of cloud amounts and types during the period from 3 to 11 Sept. 1980, and the results were acceptable.

1. Introduction

Cloud information, such as cloud amount, cloud height and cloud type have been considered as important and essential parameters in meteorology and climate. Clouds take part in the water circulation process by condensing water vapor converged from the environment and then precipitating it out of the clouds. Clouds also affect the energy budget by reflecting solar radiation, absorbing the long wave radiation from the earth and lower atmosphere and releasing the latent heat of condensation. Cloud information can be looked on as parameters for rainfall information which can be used for rainfall estimation from satellites.

Cloud observations have been made routinely from surface observational stations. But they can not provide accurate information about middle and high clouds when the low cloud cover is significant. Their space representiveness, especially over the ocean, is insufficient because of sparse island-located meteorological observational stations and ships.

Since the launch of the first meteorological satellite TIROS-1, satellite imagery data have been used broadly to derive meteorological information. The observation made by a satellite has the advantages of nearly uniform space resolution and wide scope. By use of the network comprised of polar-orbited and geostationary satellites, nearly global observation can been made at 30 minute intervals. However, there has been no method, until now, to derive cloud amount and type with acceptable accuracy and on a completly objective base, perhaps because of the characteristics of satellite observation and the enormous amount of data to be processed.

Most techniques for cloud amount estimation with meteorological satellite imagery data use IR blackbody temperature and/or albedo histograms for the area of interest. Koffler, *et al.*[1] investigated method for estimating high, middle and low cloud amounts with TIROS IR imagery data. Every pixel is assigned to clear sky,

low cloud, middle cloud or high cloud according to T_{BB}, being the surface temperature T_{SFC}–5k, 700 mb temperature (T_{700}), 400 mb temperature (T_{400}) or lower. The high, middle and low cloud amounts for a 32 line $\times$32 pixel area are then defined as the ratioes of high, middle and low cloud pixel numbers to the total pixel number of the area, respectively. Meteorological Satellite Center of Japan calculates high and low cloud amounts routinely using T_{SFC}–5k and T_{400} as thresholds.

The cloud amount estimation methods mentioned above define a pixel as being clear sky or totally cloud covered from observation and by a single threshold value (hereafter referred to as Single Threshold Method, STM). It is thought that the estimations by STM may have some error arising from the use of a fixed threshold and the existence of partially cloud covered pixels, and that this error may be relatively large in estimation from large size pixels such as infrared data of geostationary satellites.

Meanwhile, the cloud type is classified from satellite imagery data operationally by trained meteorologists at present. It is clear that it is difficult for such a subjective method to make a fine cloud map (nephanalysis map) for a wide area (e.g. the whole globe) on a real time base. Aiming to solve this problem, objective cloud type classification methods have been investigated by using threshold, clustering and discriminant analysis techniques.

The threshold technique, as described by Koffler *et al.*[1] and Liljas[2], classifies cloud type according to the cloud top temperature or albedo by use of T_{BB} and/or albedo thresholds. Clustering technique, as described by Desbois *et al.*[3] and Seze and Desbois[4], classifies "similar" pixels in an interest area into several clusters. Relatively long computation time is consumed for repeating the calculation and the resulted clusters must be related to real cloud types.

The discriminant analysis technique, as investigated by Harris and Barrett[5], Parikh[6], Parikh[7] and Parikh and Ball[8], classifies an observed satellite parameter $\boldsymbol{X}$ for interest area by comparing the probabilities of $\boldsymbol{X}$ being produced by each cloud type. It is considered as a relative appropriate method for objective cloud type classification, because only simple computation is needed to classify cloud type after the cloud types to be classified are determined, the training cases for every type were selected based upon the ground truth and the discriminant equations were established.

The present paper describes a two threshold method (hereafter referred to as TTM) to estimate total cloud amount taking account of the spectral peaks due to the ground surface as well as the pixels partially covered by cloud. We will also describe a discriminant method to classify four cloud types, in relation to the future rainfall estimation, employing the data of the geostationary meteorological satellite GMS.

2. Data

In order to develop the cloud amount estimation and cloud type classification

methods, six flat areas of about 10^4 km^2 in Japan were selected as the testing areas. The IR and VIS imagery data of GMS for these six areas were collected, and the simultaneous cloud information (total cloud amount and cloud amounts for each cloud form) of the meteorological stations were collected and used as the ground truth for the periods 3 to 10 Sept. 1980, 23 July 1982 and 22 to 23 July and 7 to 9 Aug. 1983.

Fig. 1 shows the six testing areas: Hokkaido, Kanto, Kinki, Setonaikai, Sanin and Kyushu, the lengths (NS direction) and widths (EW direction) of which were respectively 80 and 110 km on average. There are four or five meteorological stations in each area. The pixel numbers are about 550 and 4400 for IR and VIS in each area.

GMS observes the earth's atmosphere by visible and infrared spin scan radiometer (VISSR) which has two observation channels of VIS (0.5–0.75 μm) and IR (10.5–12.5 μm). It had been observing routinely at an interval of 3 hours until 1986. In order to compare the satellite data with the ground observations which are made at intervals of 6 hours for most meteorological stations, only the data sets for 00Z, 06Z and 12Z could be used in this study.

VIS and IR imagery data of the six testing areas were extracted from the GMS original MT. The line and pixel numbers in the GMS imagery frame corresponding to the latitudes and longitudes of four corners of the testing area were calculated by applying a navigation method which makes a correction with the earth's edge in the image frame (Takahashi[9]).

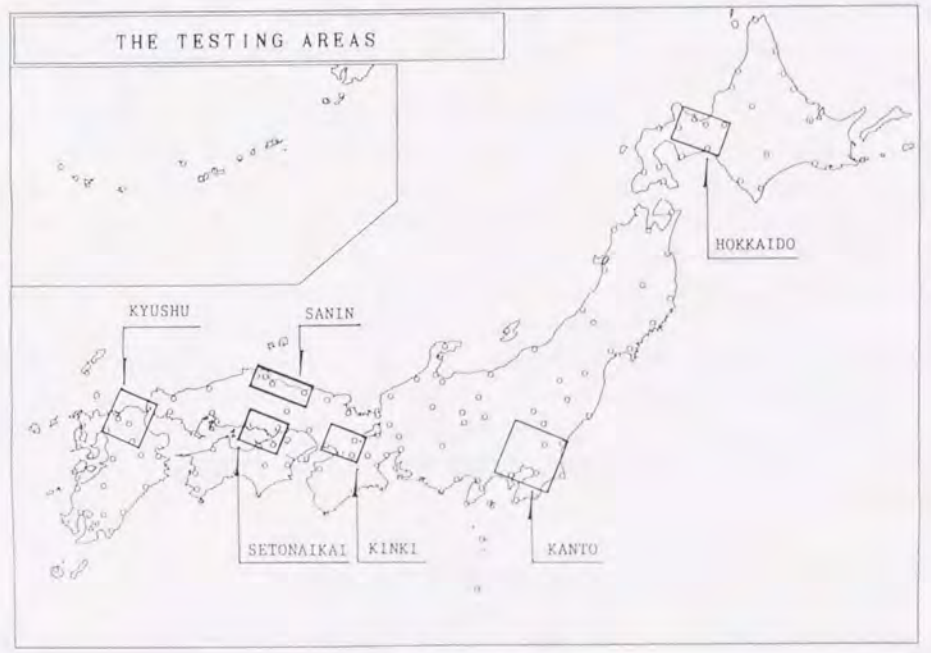

Fig. 1. The testing areas.

The extracted VIS and IR data are converted to albedo, A and blackbody temperature, T_{BB}. The conversion from IR digital count (DC) to T_{BB} can be accomplished using the calibration table which is recorded on the top of the original VISSR MT. As for the method converting VIS DC to albedo, the calibration table recorded on the MT is for the illumination condition that the sun and the satellite are both right above the reflector (e.g. clouds), it is necessary to normalize the observed albedo, a considering the solar and the satellite zenith angles, as follows:

$$A = \frac{a}{\cos Z \cdot \cos \theta} \tag{1}$$

$$\cos Z = \sin \phi \cdot \sin \delta \cdot + \cos \phi \cdot \cos \delta \cdot \cos t \tag{2}$$

$$\cos \theta = \frac{1}{(1+\tan^2 \theta)^{1/2}} \tag{3}$$

$$\tan \theta = \frac{\sin \delta}{\cos \delta - \dfrac{R}{R+H}} \tag{4}$$

$$\cos \delta = \cos \phi \cdot \cos (\lambda_s - \lambda) \tag{5}$$

where, A is normalized albedo, Z solar zenith angle, θ satellite zenith angle, ϕ and λ latitude and longitude of the observed point, δ solar declination, t hour angle, λ_s latitude of the sub-satellite point, R radius of the earth and H being the height of the satellite.

The ground truth of total cloud amounts and cloud amounts of each cloud form of the testing areas were obtained as the area weighted mean of the observed values at each station in the areas.

Cloud observation from the surface has some limitations: 1) observation extent is restricted by obstacles (e.g. mountains, high buildings) in the field of view; 2) only the clouds within a range of about 20–30 km can be observed even when there is no obstacle; 3) the visual size varies with the angle of view; 4) upper clouds can not be observed when the lower clouds are prominent and 5) the reliability declines when illumination conditions are bad (e.g. at night). In the present study, because averages of 4–5 station observations are used as the ground truths for each area of about 100 km × 100 km on plain, 1), 2) and 3) can be disregarded. Such averages are expected to give relatively reliable ground truth for cloud information.

Included among the data used in this study are, 3–11 Sept. 1980 for typhoon T8013, 23 July. 1982 for heavy rain in Nagasaki, 1–3 Aug. 1982 and 7–9 Aug. 1983 for typhoons.

3. Cloud Amount Estimation from Satellite Data

Shenk and Salomoson[10] simulated the effects of spatial resolution of the sensor on the cloud amount estimation, and showed that, in order to estimate cloud amount

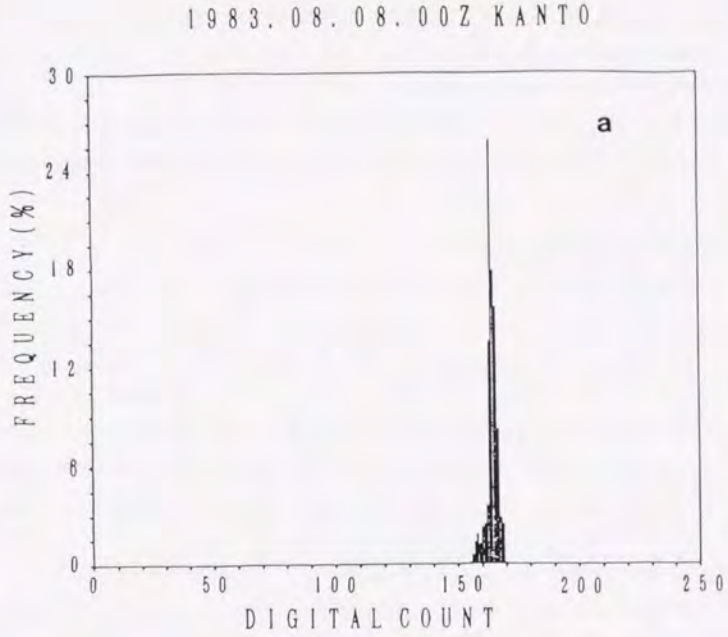

Fig. 2. The example of frequency distribution of a) T_{BB} and b) albedo, for the case of clear sky. T_{BB} 220k, 240k, 260k, 280k and 300k correspond to digital counts 46, 68, 96, 132 and 176, respectively in a). The albedo values have been normalized by considering the solar and satellite's zenith angle.

within an accuracy of 10%, the cloud size to pixel size ratio should be greater than 100 when STM is used. In the case of GMS, as the pixel size for IR is about 7 km near Japan and cloud size may be in the order of 10 km, it is difficult to satisfy this ratio. Therefore, TTM was introduced as stated before. In this chapter, after a simple analysis of T_{BB} and A histograms, the TTM, two-threshold cloud amount estimation method, was developed using satellite and surface observation data of 00Z and 06Z.

3.1 Examples of Histograms

Among the total of 156 cases of 00Z and 06Z data used here, 6 cases are with no ground observed cloud amount (clear sky case). **Fig. 2** shows an example of T_{BB} and albedo histograms for clear sky. The T_{BB} and albedo histograms have shape mono-mode distributions and concentrate in warm (T_{BB}) or dark (albedo) side. The investigation of the histograms for the six clear sky cases shows that, while the modes of T_{BB} differ from each other because of the different surface temperatures, the variation in the modes of albedo is not so large. The standard deviation of T_{BB} in a testing area ranges from 1.0°C to 3.2°C with an average of 2.0°C, and the standard deviation of albedo ranges from 0.02 to 0.05 with an average of 0.04.

Fig. 3 shows an example of T_{BB} and albedo histograms for the case of ground-observed cloud amount of 5. The ground observation shows the existence of middle clouds. The T_{BB} and albedo histograms have a warm or dark peak related to the surface while other points distribute to the cold and bright side showing the second peak corresponding to the middle clouds. When the area is overcast with clouds, the T_{BB} and albedo histograms tend to extend to the cold and bright sides, and the distribution pattern differs with cloud type. **Fig. 4** shows an example of T_{BB} and albedo histograms for the convective cloud case with total cloud amount of 10.

3.2. Cloud Amount Estimation by TTM

Based upon the above results, a two-threshold cloud amount estimation method (TTM), taking account of the spectral peaks due to the ground surface and of the pixels partially covered by clouds, was developed for daytime observations (00, 06Z). A simple schematic explanation of TTM is given in **Fig. 5**.

(a) IR Histogram

IR imagery data are the only data that can be obtained throughout the day but they have the shortcoming of poor spatial resolution. When the IR 1-dimensional histogram of the area is constructed as in **Fig. 5**, the two thresholds that discriminate the no-cloud, partial cloud and total clouds pixels were determined as follows.

If there is a peak on the warm side (T_{BB} near normal surface air temperature) of the IR histogram, and the peak temperature is T_G, the peak is assumed to be yielded by ground surface. In case no peak can be found on the warm side, the

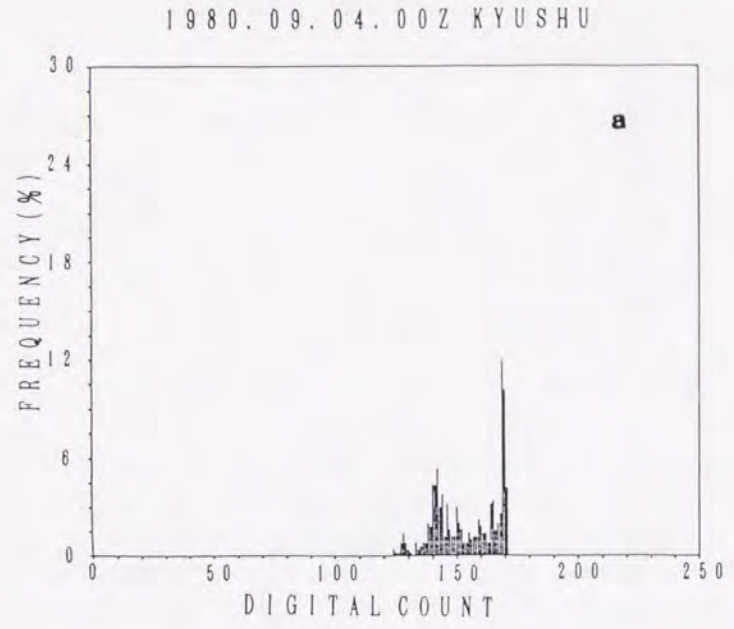

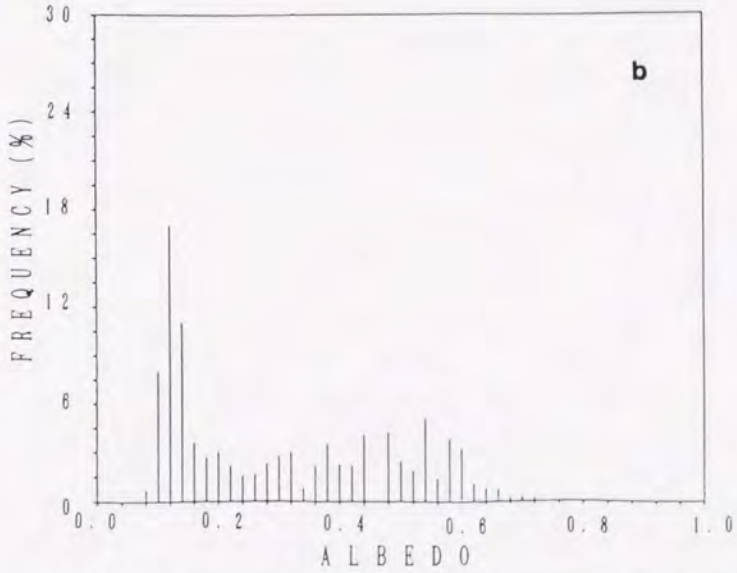

Fig. 3. As in **Fig. 2**, except for the case of total cloud amount 5. T_{BB} 220k, 240k, 260k, 280k and 300k correspond to digital counts 51, 74, 105, 143 and 189, respectively in a).

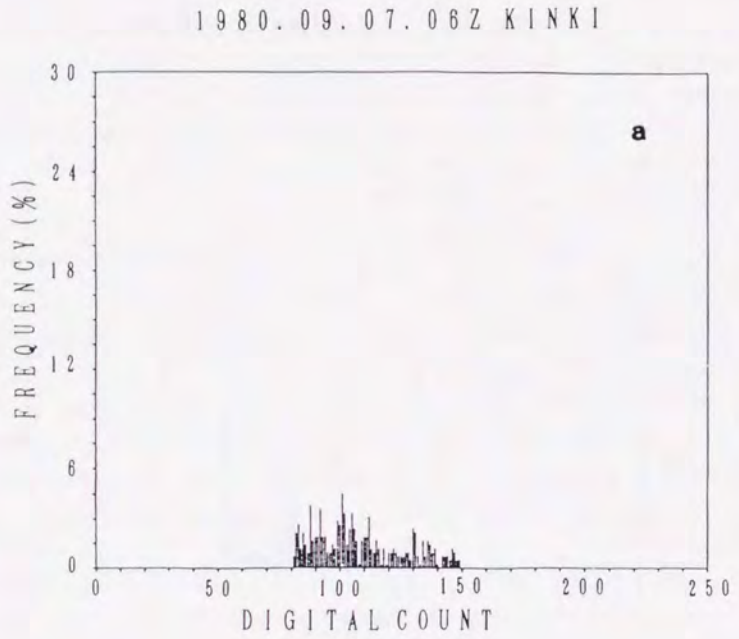

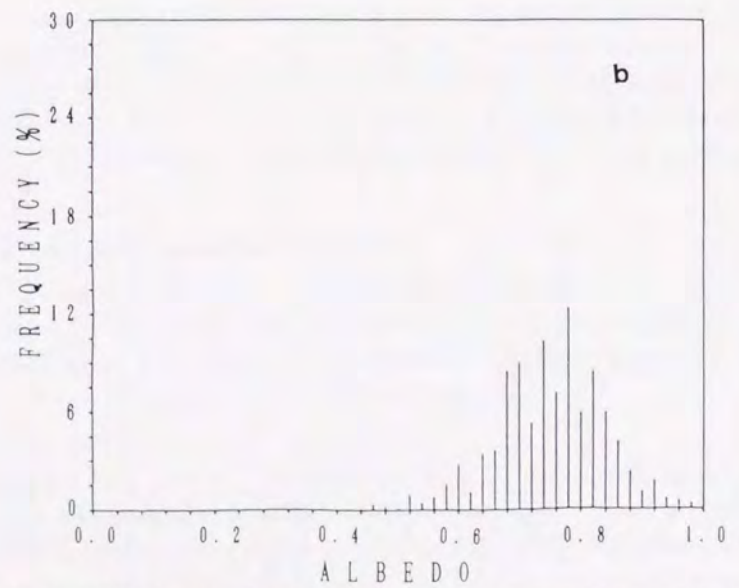

Fig. 4. As in **Fig. 2**, except for the case of total cloud amount 10 (convective cloud). T_{BB} 220k, 240k, 260k, 280k and 300k correspond to digital count 51, 74, 105, 143 and 189, respectively in a).

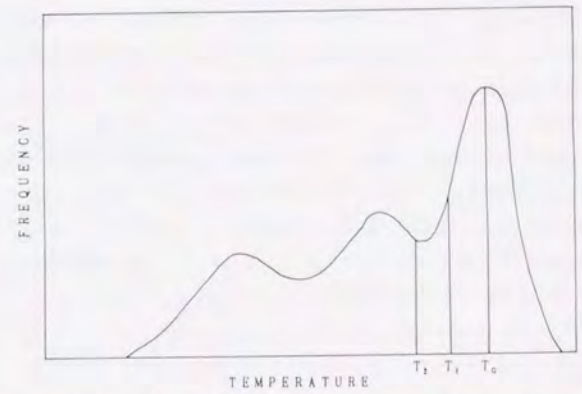

Fig. 5. Schematic figure of the two-threshold cloud amount estimation method (TTM) from T_{BB} histogram.

average of T_G of those cases with a ground peak at the same hour at the same place is used. As described above, the standard deviations of T_{BB} in the investigation areas for 6 clear sky cases have an average of 2.0k. When the area is partially covered by clouds, T_{BB} due to the no-cloud part (ground surface) are assumed to distribute around T_G with standard deviation the same as that of clear sky cases and a pixel with temperature warmer than $T_1 = T_G - 2.0$ k is defined as a no-cloud pixel.

If the warmest pixel covered totally by clouds is assumed to be with a T_{BB} of T_2, a pixel with a T_{BB} between T_1 and T_2 is considered to be covered partially by clouds. The ratio of clouds can be assumed to be linearly proportional to $\Delta T = T_1 - T_2$. That is, the satellite estimation of cloudiness, FC for an area is calculated by the following equations;

$$\mathrm{FC} = \frac{1}{N} \sum f_i \tag{6}$$

where

$$f_1 = \begin{cases} 1 & T_i \leqq T_2 \\ T_1 - T_i & T_2 < T_i \leqq T_1 \\ T_1 - T_2 & \\ 0 & T_1 < T_i \end{cases} \tag{7}$$

where T_i is T_{BB} of a pixel, N is the total pixel number of the area.

Because the second threshold T_2 can't be determined directly from IR histograms, it is selected by an indirect way. First, FC's for all cases are calculated from IR histograms by assuming various values of T_2. Regressions between the surface observed cloud amounts (GC's) and FC's for various T_2 are made and T_2 with the highest correlation coefficient is selected as the second threshold which discriminates the partial cloud and total cloud pixels. The correlation coefficients vary from 0.810 to 0.861 when $\Delta T = T_1 - T_2$ varies from 1.0k to 10.0k, with the

highest value at ΔT=1.0k. The correlation coefficient becomes 0.853 for ΔT=0.0, namely the STM case. Although the difference between correlation coefficients for TTM and STM cases was not so large, it is considered that the small difference results from the dominant cases of overcast and the cloud amount estimation is improved for the partial cloudy case. The two threshold cloud amount estimation method developed by Parikh and Ball[8] for GATE uses the warmest peak temperature as T_1, the second warmest peak temperature as T_2, and the difference between the so defined T_1 and T_2 has an average of about 2.5k, which is close to the corresponding value of 3.0k (ΔT+2.0k) in the present method. Although ΔT is calculated here from limited data and the value can be different for other areas or seasons, the method to determine it could be applicable for any case.

(b) VIS Histogram

Although VIS data can be used only in daytime and complicated normalization has to be performed, they are still considered as an important information source because of their fine spatial resolution. Similarly for IR data, when a VIS 1-dimensional histogram is used to estimate cloud amount, first of all the ground surface related peak is detected in the dark side of the histogram and in the peak albedo A_G. The first threshold $A_1=A_G+0.04$ is then determined in the same way as IR data. Assuming the second threshold has a value of A_2, the satellite estimation can be calculated by using eqs. (6) and (8).

$$f_i=\begin{cases}1 & A_i\geqq A_2\\ \dfrac{A_i-A_1}{A_2-A_1} & A_2>A_i\geqq A_1\\ 0 & A_1>A_i\end{cases} \tag{8}$$

Here A_i is the normalized albedo of a pixel. And in the same way as IR, the second threshold value A_2 is determined as $A_2=A_1-0.02$ with a correlation coefficient of 0.825.

(c) IR·VIS 2-Dimensional Histogram

Although the estimation from IR or VIS histograms has an advantage of simplicity, a relative larger error will result, because the very low clouds and thin cirrus can hardly be detected from IR or VIS data. Takeda and Hattori[11] indicated that when IR data of NOAA with spatial resolution of 1 km are used to estimate cloud amount over the ocean, the low level clouds can be detected by incorporating spatial distribution information of T_{BB} (such as standard deviation around a pixel). But no obvious improvement can be achieved when their method is applied to the IR data of GMS with a spatial resolution of 5 km. Meanwhile, as was shown by Xie and Mitsuta[12] it is possible to detect low level clouds and thin cirrus by using IR·VIS 2-dimensional histograms.

The procedures for the 2-dimensional histogram method are the same as those for the 1-dimensional one described above, except that 1) the corresponding 2 thresholds are constituted by 2 perpendicular lines in a IR·VIS domain, 2) the satellite estimation FC is calculated by eqs. (6) and (9).

$$f_i=\begin{cases}1 & T_i\leqq T_2 \text{ or } A_i\geqq A_2\\ \dfrac{T_1-T_i}{T_1-T_2} & T_2<T_i\leqq T_1,\ A_1>A_i\\ \dfrac{A_i-A_1}{A_2-A_1} & T_1<T_i,\quad A_2>A_i\geqq A_1\\ \mathrm{MAX}\left[\dfrac{T_1-T_i}{T_1-T_2},\ \dfrac{A_i-A_1}{A_2-A_1}\right] & T_2<T_i\leqq T_1,\ A_2>A_i\geqq A_1\\ 0 & T_1<T_i,\quad A_1>A_i\end{cases} \tag{9}$$

Here, T_i and A_i are the T_{BB} and albedo of pixel, $T_1=T_G-2.0$k and $A_1=A_G+0.04$ are the first thresholds to discriminate clear sky and partial cloud pixels. The statistical results showed that the highest correlation coefficient of 0.889 is obtained when $T_2=T_1-2.0$k and $A_2=A_1-0.04$.

3.3 Comparison of Satellite Estimated Cloud Amounts and Ground Observations

The cloud amount estimation methods described above were tested and compared with the corresponding ground observations. Comparisons were made for daytime (00Z, 06Z) data which were used in the development of the method, and nighttime (12Z) with the same methods, respectively.

The satellite estimated FC's were calculated from IR, VIS 1-dimensional histograms and IR-VIS 2-dimensional histograms separately by using thresholds determined in the preceeding section. **Fig. 6** gives a comparison between IR estimated FC's and ground observed GC's for the daytime. The points were scattered when ground cloud amounts were 4–6. The correlation coefficient between FC's and GC's is 0.861 and the RMS error for FC's was 0.155. Kubota and Endo[13] estimated the cloud amounts for a $1^\circ\times1^\circ$ area by using GMS IR imagery data in a one threshold method, defining the cloud pixels as 5°C colder than the surface temperatures defined by the GMSSA climate data. Their comparison between the estimated values and the ground observations showed a correlation coefficient of 0.438 and RMS error of 0.331 for overland cases. Although no direct comparison can be made between the results in their and the present study because different data are used, significant difference in corelation coefficients in the two studies implies that TTM developed here did improve cloud amount estimation.

The comparisons between VIS estimated FC's and GC's, IR-VIS estimated FC's and GC's were also conducted for the daytime. The correlation coefficients and RMS errors were 0.825 and 0.167 for VIS estimations, and 0.889 and 0.140 for IR-VIS two dimensional estimations. It was found from the comparisons that the best correspondence between FC's and GC's is obtained when both IR and VIS data are

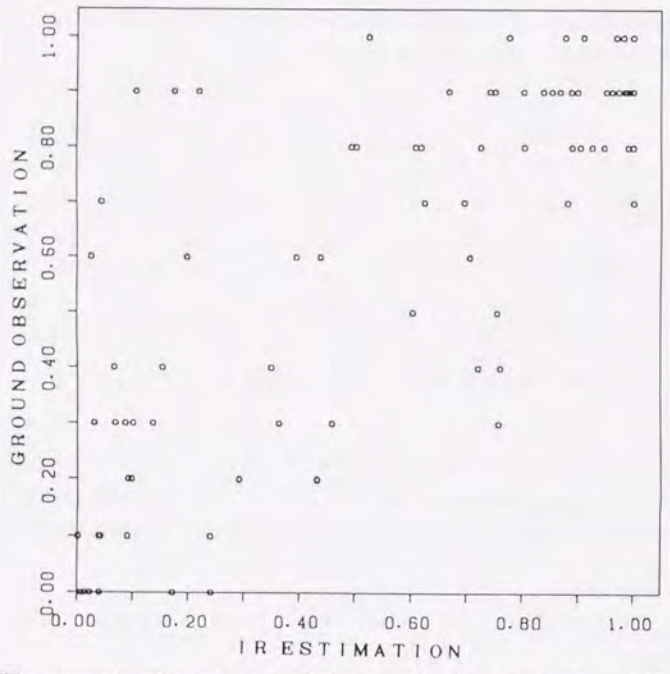

Fig. 6. The comparison between ground observed cloud amounts GC and IR derived fractional coverages (FC) by use of the two-threshold cloud amount estimation method (TTM) for 156 daytime cases. GC and FC are indicated in the range of 0–1.

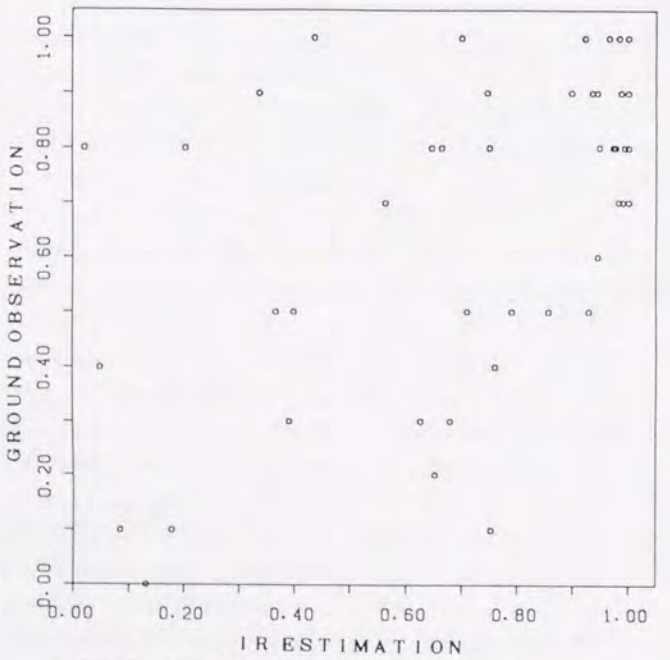

Fig. 7. As in **Fig. 6**, except for 84 nighttime cases.

used, but the differences from other methods are not so large.

The IR cloud amount estimation method developed with the daytime data was applied to estimate the nighttime cloud amounts with the same methods and the results were compared with the surface observations for 84 cases of 12Z. **Fig. 7** shows the scatter diagram of IR estimated and surface observed cloud amounts. In general, the IR estimations were overestimated compared to the surface observations, the correlation coefficient was 0.659, and lower than that for the daytime (0.861). It is considered that the reduction of the coefficient results from an error of ground temperature T_G when cirrus clouds present and errors in observation of clouds from the surface at night.

4. Cloud Type Classification

As described in the introduction, discriminant analysis technique is considered as the most appropriate one for objective cloud type classification among the three methods. In this section, such a method is developed to classify the cloud type for the 6 test areas by using GMS imagery data. Although similar methods have been investigated by several authors (e.g. Parikh and Ball[8]), it is still necessary to apply and test the technique to classify cloud types defined for rainfall estimation, and to attempt to get the best results by trying to select the most effective parameters from the various satellite parameters used and unused in previous studies.

As described by Okuno *et al.*[14] and Sugiyama[15], discriminant analysis technique classifies cloud types as follows: assuming there is a total number of p parameters which characterize cloud type i out of n, and the observed vector $\boldsymbol{X}$ of cloud type parameters is obtained, the probability to obtain $\boldsymbol{X}$ when cloud type is i, $Pr(\boldsymbol{X}\,|\,i)$, becomes as follows, assuming the p-th degree normal distribution for $Pr(\boldsymbol{X}\,|\,i)$;

$$Pr(\boldsymbol{X}\,|\,i) = \frac{1}{(2\pi)^{p/2}\,|\,\boldsymbol{\Sigma}\,|^{1/2}} \times \exp\left[-\frac{1}{2}\,(\boldsymbol{X}-\boldsymbol{M}_i)^T\,\boldsymbol{\Sigma}^{-1}(\boldsymbol{X}-\boldsymbol{M}_i)\right] \tag{10}$$

where $\boldsymbol{M}_i$ is the mean vector for cloud type i and the covariance matrix $\boldsymbol{\Sigma}$ is assumed to be equal for every cloud type. The discriminant analysis technique assigns a satellite observation with parameter vector $\boldsymbol{X}$ to cloud type j, when

$$Pr(\boldsymbol{X}\,|\,j) > Pr(\boldsymbol{X}\,|\,i)\,, \quad \text{for all} \quad i \neq j \tag{11}$$

A cloud type classification method was thus developed by using GMS IR and/or VIS imagery data for 00Z and 06Z and the classification results were evaluated by the comparison with the cloud types obtained from the ground.

4.1 Determination of the Cloud Types

The cloud types to be classified are different case by case according to the purpose of the study. Koffler *et al.*[1] classified 3 cloud types based on the cloud top temperatures. Liljas[2] identified 6 cloud types according to the temperatures and

Table 1. Criteria for selection of the cloud type classification training cases

Cloud Type		Number of Selected Case	Selection Criteria
Sign	Name		
A	Cumulus	18	NT=10, Cu>7, No Cb
B	Cumulonimbus	9	NT=10, Cb>5
C	Middle Cloud	28	NT=10, As+Ac>7, No Cb
D	High Cloud	15	NT=10, Ci+Cs+Cc>7, No lower cloud

albedos of the clouds. Harris and Barrett[5] classified surface and 4 cloud types: stratiform, stratocumulus, mixed and cumulus clouds. Pairkh[6] discriminated 4 types of low clouds, mixed clouds, cumulonimbus and cirrus. He later[7] divided cirrus clouds into cirrus unmixed with other clouds and cirrus mixed with other clouds. Parikh and Ball[8] designed a method for classifying 5 types: low clouds only, middle clouds with no significant high clouds, high clouds with no significant lower clouds, high clouds with significant lower clouds and Cb.

In the present study, 4 cloud types as defined in **Table 1** were chosen for classification, considering the future application of the discriminant results to the rainfall estimation technique. In **Table 1**, type A, B, C and D denote cumulus, cumulonimbus, middle clouds and high clouds, and NT, Cu, Cb etc. are total cloud amount and cloud amounts for every cloud form observed from the surface, respectively. 70 cases (training cases) that satisfy the selection criteria described in **Table 1** were selected from the 156 cases of 00Z and 06Z based upon the ground observed cloud types, and used to develop the cloud type classification method. Among the 70 selected cases, type A, B, C and D include 18, 9, 28 and 15 cases, respectively.

4.2 Method of Classification

264 parameters for classifying the cloud types were selected and calculated from the total histograms, quadrant histograms, difference histograms[6),7)] and Roberts Gradient histograms[8)] of IR and VIS imagery data. 80 of them are spectral parameters reflecting ground or cloud information such as mode, mean, maximum and minimum, and 184 of them are textural parameters reflecting ground or cloud smoothness information.

The best combinations for classifying the 4 cloud types were then selected from the calculated 264 parameters by using the forward selection technique described in Okuno *et al.*[14)] and Sugiyama[15)]. As a result, it was revealed that 1) the best classification results are obtained when both IR and VIS parameters were used, and the worst results appeared when only IR parameters were used, 2) better classification resulted using more parameters but the improvement becomes less significant when more than 4 parameters were used. The selected best 4 parameter combination for IR data is given in **Table 2** and $TBB_{0\%}$, $TBB_{10\%}$, $TBB_{50\%}$ and $TBB_{90\%}$ are TBB values at 0%, 10%, 50% and 90% points in a cumulated TBB histogram,

Table 2. Combination of selected IR parameters

No.	Parameter Definition
1	Coefficient of Variation (S.D./Mean)
2	$TBB_{90\%}$—$TBB_{10\%}$
3	$TBB_{50\%}$—$TBB_{0\%}$
4	90% Value in Roberts Gradient Histogram

respectively.

The 4 parameters selected for IR, VIS and IR and VIS were used to classify the 4 cloud types. On the assumption that the observed parameters follow the 4-dimensional normal distributions and have an equal covariance matrix, discrimination of cloud type was made consequently by comparing the values, D_i for every cloud type. $\boldsymbol{X}$ was then assigned to the cloud type j with the maximum D_i,

$$D_i = \frac{1}{2}\boldsymbol{X}^T\boldsymbol{\Sigma}^{-1}\boldsymbol{M}_i + \frac{1}{2}\boldsymbol{M}_i^T\boldsymbol{\Sigma}^{-1}\boldsymbol{X} - \frac{1}{2}\boldsymbol{M}_i^T\boldsymbol{\Sigma}^{-1}\boldsymbol{M}_i \qquad (12)$$

From the values of $\boldsymbol{\Sigma}$ and $\boldsymbol{M}_i$ calculated for the parameters of the selected 70 training cases of 00Z and 06Z, the coefficients on the right side of eq. 12 (classification equations) were determined. Cloud type classification was then made simply by substituting the observed parameter values into the equations.

4.3 Results of Classification

The cloud type classification method was then applied to classify cloud types for all cases of 00Z and 06Z, including the cases in which cloud type was not clearly defined.

The additional cases, in which ground observed cloud type was not clearly defined as shown in **Table 1**, were classified into additional categories as shown in **Table 3**. Type S (clear sky) are those with cloud amounts smaller than 0.3, Type F (fraction) are those with cloud amounts GC 0.4–0.6, and Type MA (Mixed A), MB (Mixed B), MC (Mixed C) and MD (Mixed D) are those with cloud amounts over 0.7 and covered mainly by the clouds of Type A, B, C and D but not defined as A, B, C and D in **Table 1**.

The satellite cloud type classification was performed in two steps. At first, the cloud amount was estimated by using TTM described in Chapter 3. The cases having cloud amount estimations smaller than 0.3 and 0.7 were then classified as Type S and F, respectively. Secondly, the classification equations described in (4.2) for 4 types were then applied to the cases with cloud amounts not smaller than 0.7.

Table 3 shows the comparison of the results of satellite classified cloud types using IR parameters with the ground observed data. Among the 70 training cases, 5 cases were classified as Type F, 37 cases were classified correctly, giving a correctness ratio of 52.9%. Among the 50 mixed cloud cases, 5 MA cases, 2 MB cases,

Table 3. Cloud type classification result from IR data for daytime

Type	Discriminated Type						
	S	F	A	B	C	D	Total
S	20 (83.3)	2 (8.3)	0 (0.0)	0 (0.0)	2 (8.3)	0 (0.0)	24
F	4 (33.3)	4 (33.3)	0 (0.0)	0 (0.0)	4 (33.3)	0 (0.0)	12
A	0 (0.0)	0 (0.0)	11 (61.1)	0 (0.0)	7 (38.9)	0 (0.0)	18
B	0 (0.0)	1 (11.1)	2 (22.2)	4 (36.4)	1 (11.1)	1 (11.1)	9
C	0 (0.0)	2 (7.1)	15 (53.6)	0 (0.0)	11 (39.3)	0 (0.0)	28
D	0 (0.0)	2 (13.3)	0 (0.0)	0 (0.0)	2 (13.3)	11 (73.3)	15
MA	2 (14.3)	3 (21.4)	5 (35.7)	1 (7.1)	1 (7.1)	2 (14.3)	14
MB	1 (33.3)	0 (0.0)	0 (0.0)	2 (66.7)	0 (0.0)	0 (0.0)	3
MC	1 (5.9)	0 (0.0)	1 (5.9)	5 (29.4)	8 (47.1)	2 (11.8)	17
MD	0 (0.0)	3 (18.8)	2 (12.5)	2 (12.5)	0 (0.0)	9 (56.3)	16
Total	28 (17.9)	17 (10.9)	36 (23.1)	14 (9.0)	36 (23.1)	25 (16.0)	156 (100.0)

8 MC cases and 9 MD cases were classified as Type A, B, C and D, respectively. In general, classifications of type B (Cb) and D (high clouds) matched comparatively well, but misclassification between types A (Cu) and C (middle clouds) was significant. Misclassification may result from the similarility in appearances of the two types of clouds when observed from a satellite.

The cloud type classification method developed for the daytime data were also applied to classify the cloud types for the nighttime (12Z) cases which the surface cloud observations are less reliable. The comparison between IR classified and ground observed cloud types are shown in **Table 4**. Results of classification were similar to that for the daytime cases. Among the 44 cases of cloudy condition with single cloud type, 21 cases were classified correctly and the correct ratio decreased to 47.7%, among the 23 mixed cloud cases, 3 MA cases, 2 MC caess and 2 MD cases were classified as Type A, C and D, respectively.

As seen above, cloud classification by GMS IR imagery data was acceptably good and even in mixed cloud cases, the main cloud form was detectable except for recognition of middle clouds from cumulus clouds, and vice versa.

Table 4. Cloud type classification result from IR data for nighttime

Type	Discriminated Type						
	S	F	A	B	C	D	Total
S	3 (37.5)	0 (0.0)	1 (12.5)	0 (0.0)	4 (50.0)	0 (0.0)	8
F	1 (11.1)	0 (0.0)	2 (22.2)	0 (0.0)	5 (55.6)	1 (11.1)	9
A	2 (10.0)	0 (0.0)	5 (25.0)	7 (35.0)	6 (30.0)	0 (0.0)	20
B	0 (0.0)	0 (0.0)	1 (25.0)	1 (25.0)	1 (25.0)	1 (25.0)	4
C	0 (0.0)	0 (0.0)	2 (13.3)	2 (13.3)	11 (73.3)	0 (0.0)	15
D	0 (0.0)	0 (0.0)	0 (0.0)	1 (20.0)	0 (0.0)	4 (80.0)	5
MA	0 (0.0)	0 (0.0)	3 (25.0)	3 (25.0)	6 (50.0)	0 (0.0)	12
MB	0 (—)	0 ( )	0 (—)	0 (—)	0 (—)	0 (—)	0
MC	0 (0.0)	0 (0.0)	1 (20.0)	2 (40.0)	2 (40.0)	0 (0.0)	5
MD	0 (0.0)	0 (0.0)	0 (0.0)	0 (0.0)	4 (66.7)	2 (33.3)	6
Total	6 (7.1)	0 (0.0)	15 (17.9)	16 (19.0)	39 (46.4)	8 (9.5)	84 (100.0)

5. Applications of the Cloud Amount Estimation and Cloud Type Classification Techniques

The techniques to estimate cloud amounts and to classify cloud types from GMS IR imagery data discussed in the previous sections were tested and applied to a time series of data of six testing areas for the period from 00Z Sept. 3, 1980 to 12Z Sept. 11, 1980.

The results are shown in **Fig. 8 a-f** together with ground observed data at 00, 06 and 12Z. As explained before, the satellite data were observed in 3 hour interval, instead of hourly as at present. During this period, a stationary front extended over almost the entire Japan islands from Chishima island in the direction of northeast-southwest, on Sept. 8 and Typhoon T8013 passed Kyushu Island on Sept. 10.

The cloud amount estimated from the satellite data showed good agreement with the ground observed data, if considered a significant difference of observation times between both methods. The GMS scans the vicinity of the Japanese islands about 20 min earlier than the surface observation.

The cloud type classification from satellite may be significantly in agreement with the ground observed data, except for the confusion of type A and C in satellite classifications. We could not find any significant difference in estimation score in

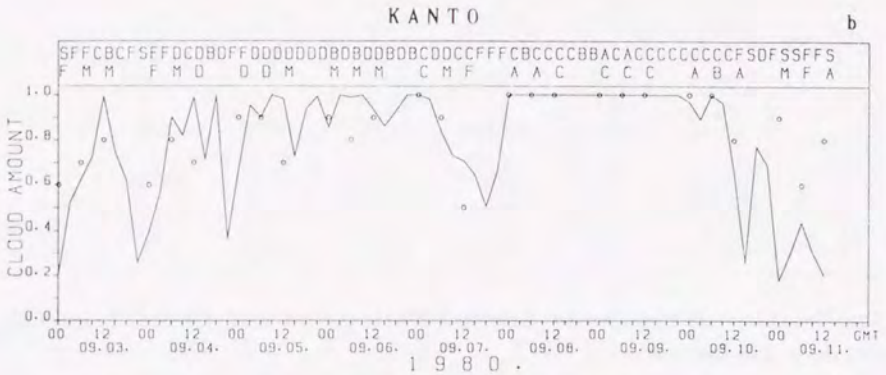

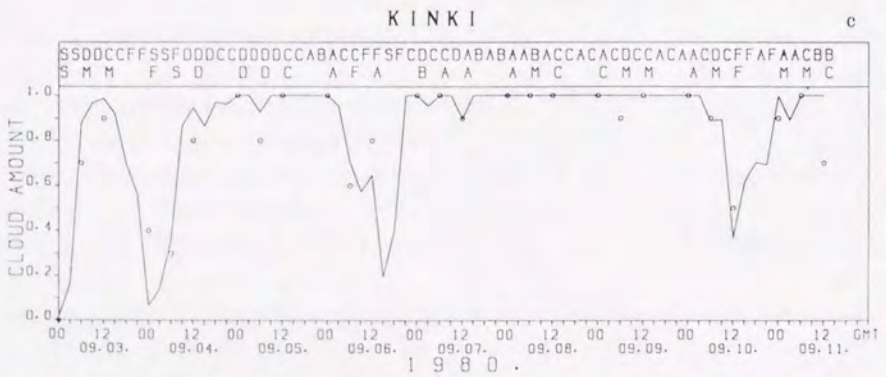

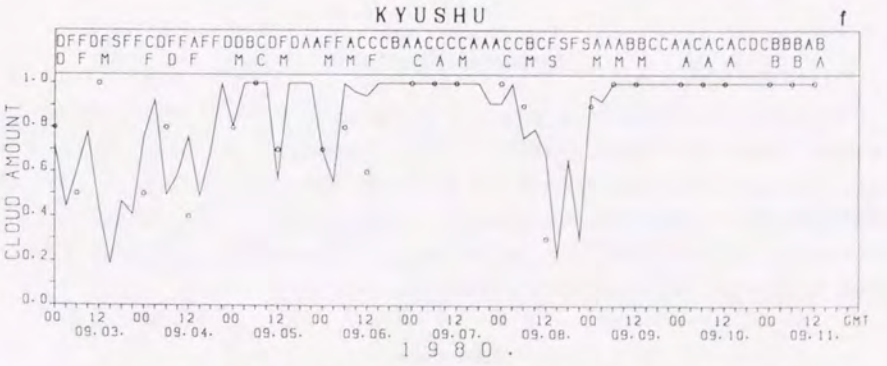

Fig. 8. Time series of IR estimated and ground observed cloud amounts and cloud types for the period of 00Z Sept. 3 to 12Z Sept. 11, 1980, for a) Hokkaido, b) Kanto, c) Kinki, d) Setonaikai, e) Sanin and f) Kyushu. The cloud amounts of ground observation and IR estimation are ploted in circles and solid line, respectively. The cloud types derived from ground observation and IR data are listed in the lower and upper lines above the cloud amounts charts. Signs of S, F, A, B, C and D denote Clear Sky, Fraction, Type A, B, C and D, respectively. Sign M includes MA, MB, MC and MD.

areal difference from Hokkaido to Kyushu.

6. Conclusions

Methods to estimate cloud amount and classify cloud type for an area of about 10^4 km^2 have been investigated by using IR and/or VIS imagery data of GMS and the surface cloud observation data as reference.

A Two-Threshold-Method (TTM) which takes account of the ground related spectral peak and of the partially cloud-covered pixels has been developed to estimate the total cloud amount from GMS IR and/or VIS imagery data. The satellite estimated and surface observed cloud amounts agree apprecicably with correlation coefficients of 0.861 and 0.659 for the daytime and nighttime respectively when IR data were used.

A discriminant analysis technique was applied to classify 4 types of clouds: cumulus, cumulonimbus, middle clouds and high clouds. Combinations of four parameters are selected to classify the cloud types. The comparisons between the cloud types classified by IR data and ground observed data show correctness ratios of 52.9% and 47.7% for the daytime and nighttime. Confusions of cumulus and middle cloud are the largest cause of misclassification.

The methods were applied to produce the time series of cloud amounts and cloud types for the period of a week by use of IR data. The satellite derived cloud amounts and cloud types showed variations corresponding to the passages of weather systems and their variation trends agree relatively well with those indicated by the surface observations.

To have more reliable classification, the methods should be improved in the introduction of time changes of images in hourly observations, as well as diminishing the effects of cirrus and distinguishing cumulus from middle cloud.

Acknowledgements

The author would like to express his thanks to Prof. Y. Mitsuta of the Disaster Prevention Research Institute (DPRI), for his continuous guidance and encouragements. The author is also grateful to Prof. M. Yamada and Mr. M. Horiguchi of DPRI, for their valuable discussions and encouragement. The computations were performed by FACOM M-730 computer at the Information Processing Center of Disaster Prevention Studies of DPRI of Kyoto University.

References

1) Koffler, R., A. G. Decotiis and K. Rao: A Procedure for Estimating Cloud Amount and Height from Satellite Infrared Radiation Data, Mon. Wea. Rev., Vol. 101, 1973, pp. 240–243.
2) Liljas, E.: Automated Technique for the Analysis of Satellite Cloud Imagery, In "Nowcasting", 1982, pp. 167–176, Acadmedic Press.
3) Desbois, M., G. Seze and G. Szejwach: Automatic Classification of Clouds on METEOSAT Imagery: Application to High-Level Clouds, J. Appl. Met., Vol. 21, 1982, pp. 401–412.
4) Seze, G. and M. Desbois: Cloud Cover Analysis from Satellite Imagery Using Spatial and Temporal Characteristics of the Data, J. Climate Appl. Met., Vol. 26, 1987, pp. 287–303.
5) Harris, R. and C. Barrett: Toward an Objective Nephanalysis, J. Appl. Met., Vol. 17, 1978, pp. 1258–1266.
6) Parikh, J.: A Comparative Study of Cloud Classification Techniques, Remote Sensing of Environment, Vol. 6, 1977, pp. 67–81.
7) Parikh, J.: Cloud Classification from Visible and Infrared SMS-1 Data, Remote Sensing of Environment, Vol. 7, 1978, pp. 85–92.
8) Parikh, J. and J. T. Ball: Analysis of Cloud Type and Cloud Amount during GATE from SMS Infrared Data, Remote Sensing of Environment, Vol. 9, 1980, pp. 225–245.
9) Takahashi, D.: Navigation of VISSR Imagery by Detecting the Earth Edge, Meteorologiacl Satellite Center Technical Report, Vol. 3, 1980, pp. 55–68 (in Japanese).
10) Shenk, W. E. and V. V. Salomonson: A Simulation Study for Exploring the Effects of Sensors Spatial Resolution, J. Appl. Met., Vol. 11, 1972, pp. 214–220.
11) Takeda, T. and F. Hattori: Analysis of Low Clouds over Sea Using NOAA Data, Preceeding of 1988 Spring Conference of JMS, 1988, pp. 30 (in Japanese).
12) Xie, P. and Y. Mistsuta: Rainfall Estimation from GMS Infrared and Visible Imagery Data, Annuals of Disas. Prev. Res. Inst., Kyoto Univ., No. 32B-1, 1988, pp. 201–217 (in Japanese).
13) Kubota, K. and A. Endo: Digitalization of Cloud Distribution, Meteorological Satellite Data and Numerical Forcasting, Report of Computer Division, No. 26, 1980, pp. 30–33 (in Japanese).
14) Okuno, M. et al.: Multivariate Analysis, Nichikagiren, 1976, pp. 299 (in Japanese).
15) Sugiyama, T.: Introduction to Multivariate Analysis, Asakurashoten, 1983, pp. 173 (in Japanese).

主論文－2

Rainfall Estimation in the Midlatitudes from GMS Infrared Imagery Data

By Pingping XIE

Reprinted from Bulletin of the Disaster Prevention Research Institute
Kyoto University
Volume 41, June, 1991

Rainfall Estimation in the Midlatitudes from GMS Infrared Imagery Data

By Pingping XIE

(Manuscript received on March 6, 1991)

Abstract

A new method is proposed for estimation of rainfall in mid-latitudinal areas from **GMS** infrared imagery data. This method was developed by using the satellite and gage data in 5 areas of about 10^4 km^2 in Japan, taking account of the different features of rainfall from various types of clouds. In this method, clouds are classified into six types, **S**(Clear Sky), **F**(Fine), **A**(Cumulus), **B**(Cumulonimbus), **C**(Middle Clouds) and **D**(High Clouds), by using the discriminate analysis technique from **IR** imagery data. The cloud types **S**, **F** and **D** are assumed to be no-rain cases and in the cases of **A**, **B** and **C**, rainfall is assumed to be proportional to the cold cloud fractional coverage (**FC**). A proportional constant for each cloud type is determined from the regression equation between **FC** and 3-hr rainfall, where the threshold T_{BB} used to define **FC** is determined to give the highest correlation for each cloud type. This method gives a good rainfall estimation for 24 hr cumulative rainfall with the correlation coefficient of 0.651 and relative root mean square error (**RRE**) of 0.968. To apply this method to the Hokkaido area, the results should be adjusted by an empirically determined factor, because weather conditions are different in this area.

1. Introduction

Investigation of the spatial distribution and time change of global rainfall is a fundamental requirement in understanding global weather systems. However, the present rainfall observation network consisting of radars and gages does not cover the oceanic area and upcountry (Browning[1]). The recent development of the meteorological satellite has enabled us to observe rainfall from space, and many methods have been proposed to estimate rainfall from infrared (**IR**) and visible (**VIS**) imagery data of meteorological satellites (*e. g.* Martin and Scherer,[2] Barrett and Martin,[3] Tsuchiya[4] and Arkin and Ardanuy[5]). Besides these methods, passive microwave radiometer and active radar observation of rainfall from satellite are also under development (Simpson *et al.*[6]). However, observation from the geosychronous satellite is the best in terms of spatial and time resolution of the global distribution of rainfall, although it has the limitation of being an indirect method.

Among the rainfall estimation techniques using geosynchronous satellite data which have been developed so far, the "life cycle" methods and the "cloud coverage" methods are typical and are considered to be relatively successful. The life cycle method, as developed by the group of Griffith and Woodley (Griffith *et al.*[7], Woodley *et al.*[8], Augus-

tine *et al.*[9], and Griffith[10]) estimates rainfall volume for individual clouds under the assumptions that: a) rainfall falls from cold clouds; b) rainfall is proportional to cloud area and c) the constant of proportionality is related to the life cycle stage of the clouds. Rainfall was then calculated from the cloud area colder than a threshold (253K in Griffith and Woodley's method) and life cycle stage parameters derived from the time series of the cloud images. In this method clouds must be tracked throughout their lifetimes on satellite images, and thus relatively complex procedures and long **CPU** time are required. However, testing the method of Griffith and Woodley with the same data, Negri *et al.*[11] found that the estimated rainfall is highly correlated with the cloud area but not so well with the parameters related to the life cycle stage, and they concluded that comparatively good estimation can be made using only appropriately defined cloud areas.

The cloud coverage method, as developed by the group of Arkin *et al.* (Arkin[12], Richards and Arkin[13], Arkin and Meisner[14], Meisner and Arkin[15] and Arkin *et al.*[16]) estimated rainfall for climatic scales ($\geq 10^4$ km^2 in space and ≥ 5 days in time) from cloud coverage colder than a threshold (235k in Arkin's method) under the assumption that the cloud life cycle effect is diminished by averaging the states in both space and time. Rainfall was then estimated from cold cloud coverage by using an empirically established linear relation between them, where the threshold temperature was determined by empirical methods.

Most of the methods described above have been developed for estimating rainfall in tropical areas, where rainfall is associated mainly with convective clouds. In mid-latitudinal areas near Japan, however, it becomes more difficult to estimate rainfall from satellite data, because precipitation from stratiform clouds and nonprecipitating cirrus clouds often appear. Wylie[17], Griffith *et al.*[18] and Arkin and Meisner[14] tried to apply the methods developed for tropical areas to estimate mid-latitudinal rainfall, and obtained reasonable success in estimating convective rainfall. However, to estimate total rainfall in mid-latitudes, it is necessary to consider various types of clouds.

Xie and Mitsuta[19] tried to distinguish cirrus that does not cause rain from other clouds by joint use of **GMS** (Geostationary Meteorological satellite of Japan) **IR** and **VIS** imagery data and to estimate hourly rainfall for the noncirrus cases by using a linear regressional equation between rainfall and cold/bright cloud coverage. Relatively good correlation ($r=0.76$) was obtained between the estimated rainfall and gage-observed rainfall. However, this method can not be applied at night, which prevents long range cumulative rainfall estimation in this method. Recently, Xie[20] developed a method for classifying six cloud types from **GMS IR** imagery data by using a discriminate analysis technique, which can be used for rainfall estimation.

In the present paper, a method applicable for both day- and night-time has been developed to estimate rainfall in mid-latitudinal areas of about 10^4 km^2 by using cold cloud fractional coverage and the cloud type classified by the method of Xie[20], and some examples of its application are shown.

2. Satellite and Gage Data

The same satellite data sets as those used in Xie[20] and gage rainfall data for the same periods are employed to develop the rainfall estimation method. These data sets are for the six testing areas of about 10^4 km^2, Hokkaido, Kanto, Kinki, Setonaikai, Sanin and Kyushu, located in plain areas in Japan (see **Fig.1** of Xie[20]). Rather large testing areas have been chosen, because Richards and Arkin[13] and Negri and Adler[21][22] have shown that good rainfall estimations in the tropics can be made from satellite **IR** data only for areas with spatial scales larger than 1.0° latitude.

The data sets consist of **GMS IR** digital data and gage-observed rainfall data for 18 days: September 3–11, 1980; July 23 and August 1–3, 1982; July 22–23 and August 7–9, 1983. The precipitation at those times was mainly due to typhoons, fronts and extratropical cyclones, respectively, and the area averaged hourly rainfall for the six areas are 0.4, 1.3, 2.7, 1.4, 1.7 and 2.0mm, respectively. Only 105 **GMS IR** images are available for these days since **GMS** observation was performed only at intervals of 3 hours in those days.

For tropical areas, Arkin[12] made use of the fractional coverage (**FC**) of cloud pixels colder than a threshold temperature from **IR** imagery for rainfall estimation. Later, Adler and Mack[23], Adler and Negri[24] and Goldenberg *et al.*[25] made use of several parameters such as minimum value and standard deviation of $\mathbf{T_{BB}}$ (Blackbody Temperature) for the tropical half hourly rain estimation for an area of 10^4 km^2, and obtained a

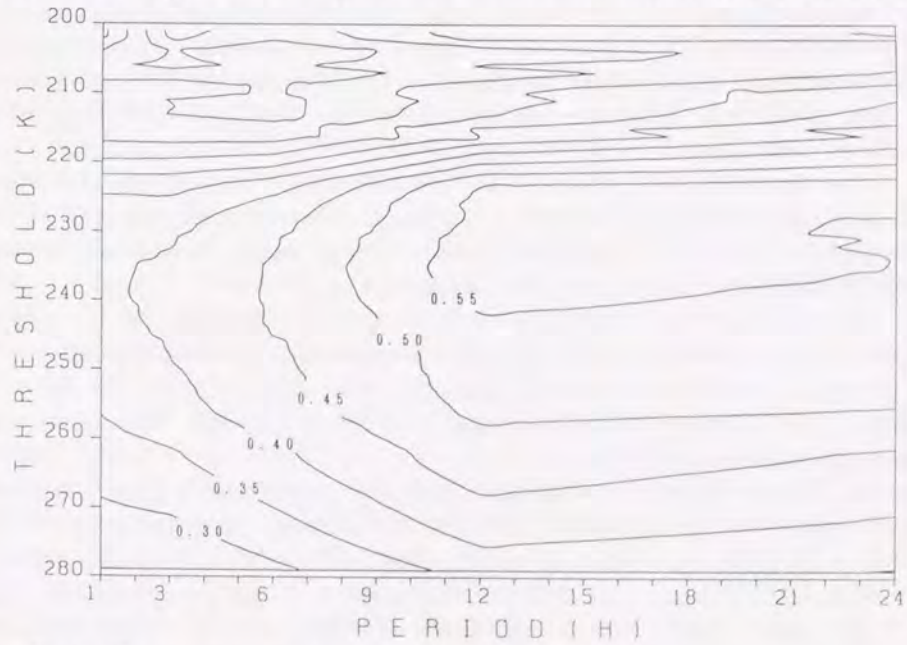

Fig. 1. The correlation coefficients between gage observed rainfall and **IR** cold cloud fractional coverage (**FC**) on various temperatures over time scale from 1 to 24 hr.

Table 1. Cloud type definition

SIGN	CLOUD TYPE	DEFINITION
S	Clear Sky	CA* < 0.3
F	Fine	0.3 ≤ CA < 0.7
A	Cumulus	CA ≥ 0.7 ; Significant Cumulus
B	Cumulonimbus	CA ≥ 0.7 ; Significant Cumulonimbus
C	Middle Clouds	CA ≥ 0.7 ; Significant Middle Clouds
D	High Clouds	CA ≥ 0.7 ; Significant High Clouds

* : Total cloud amount estimated from **GMS** infrared data by **TTM** (Two Threshold Method) as described in Xie[20].

root mean square difference of 0.39 mm from the gage-adjusted radar observation, which was only a little improvement compared to that obtained by Arkin's method (0.48) by using the same data. Also, for mid-latitudinal areas, Xie and Mitsuta[19] showed that the **FC** is useful for estimation of daytime rainfall by joint use of **IR** and **VIS** data. In the present paper, **FC** obtained only from T_{BB} histogram of **IR** data, together with the cloud type classification method developed by Xie[20], are used to estimate rainfall in the mid-latitudes.

For this reason, at first, the **IR** imagery data of the six testing areas were extracted from the original full disc **GMS VISSR** observation data, and then the T_{BB} histograms were constructed with an interval of 1K, from 200K-280K, referring the T_{BB} calibration tables. The total number of pixels for each area varies with an average of about 550.

Cloud type information is also used to discriminate the rain case and no-rain case and to estimate the rainfall caused by convective and stratiform clouds. Six types of clouds (see **Table 1** for definitions) are classified in two steps from **GMS IR** imagery data, as described in Xie [19] in detail, namely :

1) Estimate total cloud amount **CA** from **GMS** T_{BB} histograms by **TTM**(Two Threshold Method) which takes account of the ground-related spectral peak and of the partially cloud covered pixels. Define the cases with **CA** smaller than 0.3 and between 0.3 and 0.7 as Type **S**(Clear Sky) and **F**(Fine), respectively.

2) Classify clouds into four types (**A** : cumulus, **B** : cumulonimbus, **C** : middle clouds and **D** : high clouds) from the selected 4 **IR** parameters for the cloudy cases with **CA** equal to or larger than 0.7 by using the discriminate analysis technique as described by Okuno *et al.*[26] The six cloud types have been chosen to reflect the rainfall-cloud relationship in mid-latitudinal areas.

Hourly rainfall observed by **AMeDAS** (Automated Meteorological Data Acquisition System) is used as the ground truth of the rainfall. The gage distribution density of the system is about 27 km^2/gage. Although spatial variation of rainfall can be very large, the simple arithmetical average of the hourly rainfall observed by all gages located in each area is taken as the ground truth of the hourly rainfall of the area, because the gage numbers in the six testing areas (vary from 18 to 44, with an average of 25 over about 10^4 km^2) are sufficiently large and their distribution is relatively uniform. The sum of the hourly rainfalls of HH, HH+1 and HH+2 o'clocks is used as the gage observation

corresponding to the 3 hourly **GMS IR** observation of HH o'clock which scans the area near Japan on about 20 min ahead of HH.

The satellite and gage data described above are then used to investigate the relationship between rainfall and cold cloud fractional coverage (**FC**) for various types of clouds and to establish the rainfall estimation method for mid-latitudes.

3. Rainfall Estimation Method

The selection of testing areas with similar meteorological conditions is very important for developing a good empirical estimation method. A preliminary study showed that the ratios do not vary much for the testing areas except for the Hokkaido area where rainfall is much less than in the other 5 areas. For this reason, at first, the rainfall estimation method was developed by using the data of the 5 similar areas, and then the method was adjusted to estimate the rainfall for the Hokkaido area.

The correlation coefficient and relative root mean square error were used to evaluate the correspondence between gage-observed and **IR**-estimated rainfall. The correlation coefficient and the relative root mean square error (Hereafter referred to as **RRE** ; see caption in **Table 3** for definition.) were used to evaluate the similarity in temporal variability and the difference in value between the **IR** estimates and gage observations, respectively.

The possibility of applying a simple linear estimation method without regard to cloud type, such as that of Arkin, to mid-latitudinal areas, was first checked by calculating the correlations between the area-averaged rainfalls and cold cloud fractional coverages (**FC**) disregarding cloud type, for 1, 3, 6, 12 and 24 hr averages. **Fig. 1** shows the contours of the resulting correlation coefficients between rainfall and **FC** for various time scales and temperature thresholds. The correlation increased with the time scales less than 12 hr, with its maximum at the temperature threshold of 230-240k. The correlation is 0.418 for the time scale of 3 hr and 0.561 for 12 hr at the threshold of 240k. The highest correlation appears at almost the same temperatures as those in tropical areas (235K in Arkin[12], Richards and Arkin[13]). However, the poor correlation coefficients obtained indicate that it is difficult to use a simple linear relationship between rainfall and **FC** without regard to cloud type in estimatig rainfall in the mid-latitudes.

This poor correlation is considered to be caused mainly by inclusion of non-precipitating cold cirrus clouds and from disregard of different precipitating mechanisms between convective and stratiform clouds. Cloud type classified by the method of Xie[20] was thus introduced to improve the accuracy of **IR** rainfall estimation. **Fig. 2a-f** shows the scattering between 3 hr rainfall and FC at a threshold of 240k for cloud type **S**, **F**, **A**, **B**, **C** and **D**, respectively. Among the total of 72, 71 and 74 cases of cloud types of **S**, **F** and **D**, 65, 65 and 60 cases respectively show no-rain (< 1.0mm). Although no significant linear distributions could be found for the cases of cloud type **A**, **B** and **C**, their scattering concentrated mainly in the right-bottom of the figtures and made it appear that cases with larger **FC** have more rainfall on the average, suggesting a rough linear relationship between the rainfall and FC.

Fig. 2. The scattering of 3 hourly rainfall and IR fractional coverage (**FC**) at temperature threshold 240 k for the cases with cloud type a) **S**(clear sky), b) **F**(fine), c) **A** (cumulus), d) **B**(cumulonimbus), e) **C**(middle clouds) and f) **D**(high clouds), respectively.

Based upon these results, it was decided to discriminate cloud type by **IR** parameters and to estimate rainfall for the mid-latitudes as follows:

1) Discriminate the cases with cloud type of **S**(Clear Sky), **F**(Fine) and **D**(High Clouds) as no-rain cases, and other cloud types (**A**, **B** and **C**) as rain cases.

2) Estimate 3 hr rainfall for the cases with cloud type **A**(Cumulus), **B**(Cumulonimbus) and **C**(Middle Clouds) by using the linear regressional equations between 3 hr rainfall and **FC** defined by the optimal threshold for each type of raining clouds. The correlation coefficients between rainfall and **FC** at various temperature thresholds are calculated and those with the highest correlation coefficients are selected as the optimal thresholds, for the 3 types of raining clouds, respectively.

Table 2 shows the optimal thresholds and regressional equations for the 3 raining types for all 5 testing areas. Computation of respective relation for each area is difficult because of a lack of data. The optimal thresholds are 245K, 235K and 255K for type **A**, **B** and **C**, respectively. While type **B**(Cumulonimbus) has the coldest threshold and the largest proportional constant (8.460), type **C**(Middle Clouds) has the warmest and the smallest values (3.713). These differences in the thresholds and constants are characteristic if one considers the respective cloud features.

Table 2. Optimal thresholds and regression equations

TYPE	THRESHOLD	REGRESSION EQUATION
A	245 K	$E_3 = 7.582 \cdot FC$
B	235 K	$E_3 = 8.460 \cdot FC$
C	255 K	$E_3 = 3.713 \cdot FC$

E_3: 3 hr rainfall estimation

Table 3. The comparison between the **IR** estimation and gage observation*

PERIOD	KANTO	KINKI	SETONAI	SANIN	KYUSHU	5 AREAS
3 HR	0.495	0.588	0.471	0.324	0.410	0.428
	2.349	1.783	2.223	2.506	2.615	2.291
6 HR	0.537	0.651	0.526	0.391	0.592	0.516
	2.103	1.545	1.916	2.144	2.070	1.951
12HR	0.688	0.781	0.650	0.662	0.826	0.677
	1.550	1.305	1.295	1.252	1.216	1.364
24 HR	0.524	0.821	0.693	0.791	0.822	0.651
	1.487	0.848	0.938	0.765	0.853	0.968

*) The statictics on the top and bottom are correlation coefficients and **RRE** (Relative Root Mean Square Error) between the **IR** estimated and gage observed rainfall, respectively. **RRE** is defined as follows:

$$\mathbf{RRE} = \frac{[\Sigma(\mathbf{R}_i - \mathbf{E}_i)^2/\mathbf{N}]^{1/2}}{\Sigma \mathbf{R}_i/\mathbf{N}}$$

where $\mathbf{R}_i$, $\mathbf{E}_i$ are the gage observation and **IR** estimation respectively, **N** is the data number.

In order to evaluate the present method for estimating rainfall for various time scales, **IR** estimations and gage observations were accumulated and compared at 6, 12 and 24 hr. **Table 3** shows the results of correlations and **RRE**(Relative **RMS** Error) between the **IR** estimations and gage-observed rainfalls. No obvious differences can be seen among the results for the 5 testing areas. Correspondence is higher for longer time scales until 12 hr (4 images). The correlation and RRE for 24 hr estimation are 0.651 and 0.968 respectively for all the 5 testing areas. These values show improvement over the estimation which disregarded cloud type for all time scales, *e. g.* r increased from 0.561 to 0.651 for 24 hr.

Fig. 3 shows the time series of the estimations and rainfalls plotted in intervals of a) 3 hr, b) 6 hr, c) 12 hr and d) 24 hr for the Sanin area. Although the estimation fails to reflect some significant rainfall peaks caused by heavy rain, the agreement is relatively good in both variation pattern and absolute value in a time series accumulated for a long time *e. g.* for 24 hr series. **Fig. 4** shows the scattering of the **IR** estimation and rainfall for 24 hr accumulations for all of the 5 testing areas. Most of the points are distributed near the diagonal line except for one case of heavy rain in the upperleft corner, which indicates that the present method can estimate 24 hr rainfall with relatively good

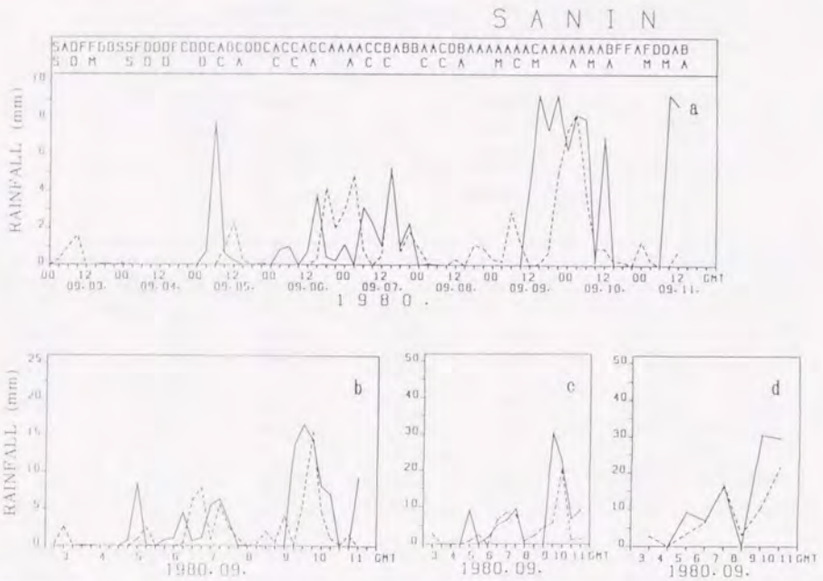

Fig. 3. Time series of the gage-observed rainfall (dashed line) and **IR** estimation (thin line), with intervals of a) 3 hr, b) 6 hr, c) 12 hr and d) 24 hr, for the Sanin area for the period from 3 to 11 Sept. 1980. The cloud types derived from surface observation and **IR** data as described in Xie[20] are also listed in the lower and upper lines above a). **S**, **F**, **A**, **B**, **C** and **D** denote Clear Sky, Fine, Type **A**, **B**, **C** and **D**, respectively. **M** includes Mixed **A**, **B**, **C** and **D**.

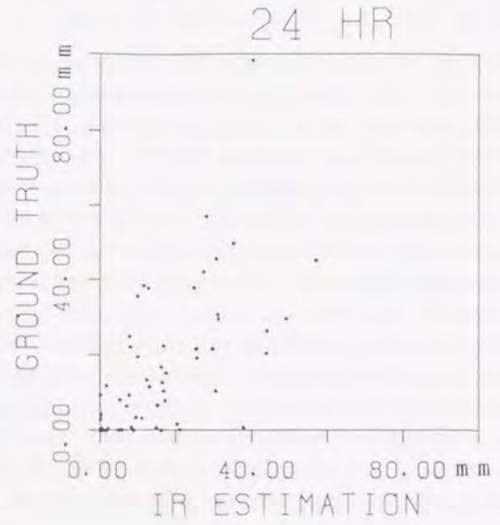

Fig. 4. Scatter plot of the gage-observed rainfall and **IR estimation for 24 hr for all the 5 areas.**

accuracy except for rain storms.

The possibility of improving the estimate by applying higher and fractional exponential equations, as well as by including other parameters such as cloud top temperature and time change of **FC** into the rainfall cloud relationship were also investigated, but no significantly improved results were obtained when compared to those obtained by using linear relations as described above.

4. Adjustment for the Hokkaido Area

When an empirically based estimation method developed for one area is applied to other areas with different weather conditions, adjustment is necessary to take into account many factors such as the environmental field or instabilities. Although attempts (Wylie[17], Alder and Mack[23]) have been made to account for these factors by using a cumulus model, it seems difficult to apply the model to an estimation area where sonde observation is rarely available. For this purpose, a simple method was tried to adjust the present method for estimating rainfall for the Hokkaido area by using the ratio of gage observation data. This adjustment method is expected to be applicable for the rainfall estimation in those marine and remote areas where at least sparse gage observation is available so that the adjustment factor for the surrounding areas can be calculated.

Fig. 5 and **Table 4** show the time series and the statistics for the comparison between the gage observed rainfall and the **IR** estimation derived by the same method for the Hokkaido area as was done in the other 5 areas. The **IR** estimation was much too high (**RRE**=5.065 for 24 hr), inspite of the relatively high correlation to the gage rainfall (r=0.780 for 24 hr). These facts suggested that the estimation could be improved by multiplying by an adjustment factor **F**(**F**<1).

In order to correct the overestimation, the adjustment factor **F** was then taken to be the ratio of the total rainfall of Hokkaido to those of the other 5 areas in the testing period, namely :

$$\mathbf{F}=\frac{\mathbf{R}_{HK}}{\mathbf{R}_{\bar{s}}}$$

where, $\mathbf{R}_{HK}$ is the total rainfall in depth for the Hokkaido area, and $\mathbf{R}_{\bar{s}}$ is the average of the total rainfall in depth for the other 5 areas used to develop the present method in the same period. The calculated value is 0.19, which indicates that only about 1/5 rainfall falls from the same cloud coverage in Hokkaido compared to the other 5 areas.

The adjustment of the rainfall estimation for Hokkaido is then made by multiplying the estimation made by the same method as for the other 5 areas by **F**(0.19). **Fig. 5** and **Table 4** show the resulting time series and the statistics of the comparison with the concurrent gage rainfall. The significant decrease of **RRE**(from 5.065 to 0.937 for 24 hr) shows the improvement achieved by the present adjustment.

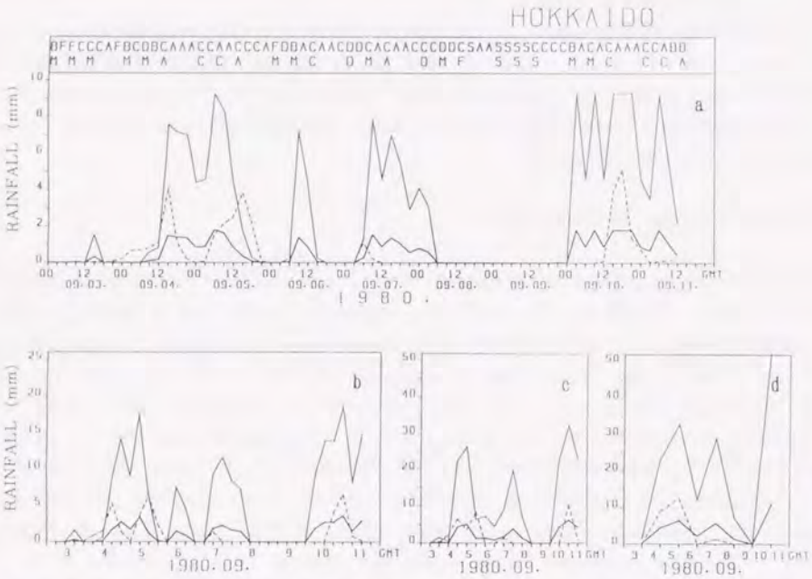

Fig. 5. As in Fig. 3, except for the gage observed rainfall (dashed line), unadjusted (thin line) and adjusted (thick line) **IR** estimation for the Hokkaido area.

Table 4 The comparison between the IR estimation and gage observation for Hokkaido area

PERIOD	UNADJUSTED	ADJUSTED
3 HR	0.456	
	8.478	2.294
6 HR	0.521	
	7.407	1.860
12 HR	0.565	
	7.213	1.591
24 HR	0.780	
	5.065	0.937

5. Conclusions

A new method has been developed to estimate the rainfall for midlatitudinal areas of about 10^4 km^2, by using the **IR** histograms and **IR** derived cloud types of the 5 areas in Japan with similar meteorological conditions with the concurrent gage rainfall data observed by **AMeDAS** as ground truth.

In order to take account of the difference of precipitating mechanisms of different types of clouds in mid-latitudinal areas, the cloud type is discriminated from **IR** parameters into **S**(Clear Sky), **F**(Fine), **A**(Cumulus), **B**(Cumulonimbus), **C**(Middle Clouds) and **D**(High Clouds). Then the cases with cloud type of **S**, **F** and **D** are assumed to be no rain cases, and estimation of the rainfall for the rest of cases is made by using the linear regressional equations between 3 hr rainfall and **FC** defined by the optimal temperature thresholds for each cloud type. The present rainfall estimation method is found to give a fairly good estimation. The 24 hr estimation shows correlation of 0.651 and **RRE** of 0.968 with the concurrent gage observation. The method is also applied to estimate the rainfall for the Hokkaido area where the weather conditions are different from the other 5 areas. While direct application resulted in a significant overestimation, the estimation was improved greatly by multiplying an adjustment factor **F** defined as the ratio of Hokkaido's rainfall to the total rainfall of the 5 other areas.

Although the present method was developed by using limited data (18 days), the relatively high correlation and small bias between the IR estimation and the gage observation suggest that it has promise for the estimation of rainfall for climatic studies. In order to validate the present method, tests are now underway by using independent data sets for various seasons and regions. Following that, the present rainfall estimation method, together with the cloud amount estimation and cloud type classification methods described in Xie[20], will be used to derive and study the spatial and temporal distribution of cloud amount, cloud type and rainfall over the oceanic areas near Japan.

Acknowledgements

The author would like to thank Prof. Y. Mitsuta of the Disaster Prevention Research Institute (DPRI) of Kyoto University, Japan, for his continuous guidance and encouragement through the work. The author is also grateful to Prof. M. Yamada of DPRI and Dr. P. A. Arkin of the office of global programs of NOAA, for their valuable discussions and comments on the manuscript. Thanks are extended to Mr. M. Horiguchi and other colleagues in the severe storm division of DPRI for their helpful discussions and encouragement. The computations are performed by FACOM M-730 computer at the Information Processing Center of DPRI of Kyoto University.

REFERENCES

1) Browning, K. A.: Rain, rainclouds and climate. Q. J. R. Meteorol. Soc., Vol. 116, 1990, pp. 1025-1051.
2) Martin, D. W., and W. D. Scherer: Review of satellite rainfall estimation methods. Bull. Amer. Meteor. Soc., Vol. 54, 1973, pp. 661-674.
3) Barrett, E. T., and D. W. Martin: The use of satellite data in rainfall monitoring. Academic Press, 1982, pp. 340.
4) Tsuchiya, T.,: Rainfall estimation methods from meteorological satellite data. Tenki, Vol. 31, 1984, pp. 607-623. (in Japanese)
5) Arkin, P. A., and P. E. Ardanuy: Estimating climatic-scale precipitation from space: a review. J. Climate, Vol. 2, 1989, pp. 1229-1238.
6) Simpson, J. A., R. F. Adler and G. R. North: A proposed Tropical Rainfall Measuring Mission (**TRMM**) satellite. Bull. Amer. Meteor. Soc., Vol. 69, 1988, pp. 278-295.
7) Griffith, C. G., W. L. Woodley, P. G. Grube, D. W. Martin, J. Stout and D. N. Sikdar:

Rain estimation from geosynchronous satellite imagery-visible and infrared studies. Mon. Wea. Rev., Vol. 106, 1978, pp. 1153–1171.
8) Woodley, W. L., C. G. Griffith, J. S. Griffin and S. C. Stromatt: The inference of **GATE** convective rainfall from **SMS-1** imagery. J. Appl. Meteor., Vol. 19, 1980, pp. 388–408.
9) Augustine, J. A., C. G. Griffith, W. L. Woodley and J. G. Meitin: Insights into errors of SMS-inferred **GATE** convective rainfall. J. Appl. Meteor., Vol. 20, 1981, pp. 509–520.
10) Griffith, C. G.: Comparisons of gage and satellite rain estimates for the centeral United States during August 1979. J. Geophys. Res., Vol. 92, 1987, pp. 9551–9566.
11) Negri, A. J., F. A. Robert and P. J. Wetzel: Rainfall estimation from satellites: an examination of the Griffith-Woodley technique. J. Appl. Meteor., Vol. 23, 1984, pp. 102–106.
12) Arkin, P. A.: The relationship between fractional coverage of high cloud and rainfall accumulations during **GATE** over the B-scale array. Mon. Wea. Rev., Vol. 107, 1979, pp. 1382–1387.
13) Richards, F., and P. A. Arkin: On the relationship between satellite-observed cloud cover and precipitation. Mon. Wea. Rev., Vol. 109, 1981, pp. 1081–1093.
14) Arkin, P. A., and B. N. Meisner: The relationship between large-scale convective rainfall and cold cloud over the western hemisphere during 1982–84. Mon. Wea. Rev., Vol. 115, 1987, pp. 51–74.
15) Meisner, B. N., and P. A. Arkin: Spatial and annual variations in the diurnal cycle of the large-scale tropical convective cloudiness and precipitation. Mon. Wea. Rev., Vol. 115, 1987, pp. 2009–2032.
16) Arkin, P. A., A. V. R. K. Rao and R. R. Kelkar: Large-scale precipitation and outgoing longwave radiation from **INSAT-1B** during the 1986 southwest monsoon season. J. Climate, Vol. 2, 1989, pp. 619–628.
17) Griffith, C. G., J. A. Augustine and W. L. Woodley: Satellite rain estimation in U. S. high plains. J. Appl. Meteor., Vol. 20, 1981, pp. 53–66.
18) Wylie, D. P.: An application of a geostationary satellite rain estimation technique to an extratropical area. J. Appl. Meteor., Vol. 18, 1979, pp. 1640–1648.
19) Xie, P., and Y. Mitsuta: Rainfall estimation from **GMS** infrared and visible imagery data. Annuals of Disas. Prev. Res. Inst., Kyoto Univ. Vol. 31B-1, 1988, pp. 201–217. (in Japanese)
20) Xie, P.,: Nephanalysis of the **GMS** imagery data. Bull. Disas. Prev. Res. Inst., Kyoto Univ., Vol. 40, 1990, pp. 57–77.
21) Negri, A. J., and R. F. Adler: Infrared and visible satellite rain estimation. part I: a grid cell approach. J. Appl. Meteor., Vol. 26, 1987, pp. 1553–1564.
22) Negri, A. J., and R. F. Adler: Infrared and visible satellite rain estimation. part II: a cloud definition approach. J. Appl. Meteor., Vol. 26, 1987, pp. 1565–1576.
23) Adler, R. F. and R. A. Mack: Thunderstorm cloud height-rainfall rate relations for use with satellite estimation techniques. J. Appl. Meteor., Vol. 23, 1984, pp. 280–296.
24) Adler, R. F. and A. J. Negri: A satellite infrared technique to estimate tropical convective and stratiform rainfall. J. Appl. Meteor. Vol. 27, 1988, pp. 30–51.
25) Goldenberg, S. B., R. A. Houze Jr., and D. D. Churchill: Convective and stratiform components of a winter monsoon cloud cluster determined from geosynchronous infrared satellite data. J. Meteor. Soc. Jap., Vol. 68, 1990, pp. 19–35.
26) Okuno, M., T. Haga, K. Yajima, C. Okuno, S. Hashimoto, Y. Furukawa: Multivariate analysis. Nichikagiren Press, 1976, pp. 299. (in Japanese)

Estimation of Rainfall on the Japanese Islands and Their Adjacent Ocean from Satellite (GMS) Infrared Imagery

By Pingping Xie

Submitted to Bull. Disas. Prev. Res. Inst., Kyoto Univ.

Abstract

The method developed for estimating rainfall over several sample areas over main islands of Japan from IR imagery data of GMS is extended to estimate rainfall over wider region including Japanese islands and their adjacent ocean. In this method, rainfall estimation over a grid of 1.25° latitudes× 1.25° longitude is made by assuming linear relations between hourly rainfall and cold cloud fractional coverage (FC) for the 3 raining cloud types (A: Cumulus; B: Cumulonimbus and C: Middle Clouds) and assuming rain free in cases of cloud amount less than 70% and cloud type D (Cirrus). The threshold temperatures to define FC for the 3 raining cloud types are kept as the same as those used in Xie[7], that is 245K, 235K and 255K for each cloud type A, B and C, respectively. The proportional constants between hourly rainfall and FC are assumed to be functions of latitude and are calculated by using the rainfall data obtained by radar-AMeDAS composite and FC data of the grids over Japanese islands. The resultant relative errors of rainfall estimation over Japanese islands are 73% and 17% for daily and monthly estimation respectively, which satisfy the useful level of the accuracy of rainfall data in climatic use.

1. Introduction

The requirements for global rainfall distribution come from many fields of meteorology and climatology. The rainfall over land can be observed directly from networks constituting of raingages and weather radars, but rainfall data over ocean are hard to obtain without the aid of satellite observation.

Among infrared(IR), visual(VIS) and passive microwave(PM) data available from the present satellite observation which can be used to detect rainfall, IR data are most hopeful in estimating rainfall for climatic scale, eventhough it is performed only by an indirect method (Barrett and Martin[1], Arkin and Ardanuy[2]). The IR techniques, such as those developed by Griffith et al.[3] and Arkin and Meisner[4], provide good estimations of rainfall in the tropical areas where convective clouds dominate. However, it is much more difficult to estimate rainfall in mid-latitudes from IR data, because non-raining cirrus and raining stratiform clouds with lower cloud tops are often observed (Xie and Mistsuta[5]). Therefore, it is necessary to introduce in the cloud type information in the rainfall estimation in mid-latitudes from satellite observed IR data.

The present author (Xie[6], Xie[7]) has developed a method to estimate rainfall in five areas of about 10^4 km^2 over the main islands of Japan from GMS (Geostationary Meteorological Satellite) IR data, using T_{BB} histogram and cloud type information derived by a discriminate analysis technique. The further step toward practical application of this IR rainfall estimation method is to adjust the method for wider area, because the method is developed originally for areas with similar weather conditions on the main islands of

Japan.

The present paper intends to extend the method for the estimation of rainfall for a region of 23.75° latitudes× 27.5° longitudes surrounding Japan with spatial resolution of 1.25° latitudes × 1.25° longitudes in June 1989.

2. Method of Rainfall Estimation

Xie[6] developed a method to estimate total cloud amount and to discriminate cloud type for areas of about 10^4 km^2 with similar weather conditions on Japanese main islands using only GMS IR data. Following to that study, Xie[7] developed a method to estimate the area-averaged rainfall for the same areas from the T_{BB} histograms and the cloud type derived from the IR data. The foundamental procedures to estimate rainfall from IR imgery data in this method are as follows;

1) Estimate total cloud amount of the target area from T_{BB} histogram by the method developed in Xie[6], which takes account of the ground-related spectral peak and the partially cloud-covered pixels. Define the case with cloud amount smaller than 0.3 as Clear Sky (Type S), that between 0.3 and 0.7 as Fine (Type F) and that equal to or larger than or 0.7 as cloudy case, respectively.

2) In cloudy case with cloud amount equal to or larger than 0.7, classify clouds into four types A:cumulus, B:cumulonimbus, C:middle clouds and D:high clouds from the selected 4 IR cloud feature parameters (see Table 3 in Xie[6]) by using discriminate analysis technique.

3) Estimate hourly rainfall for each area by using the cloud type information and T_{BB} histogram. The cases with cloud type of S (Clear Sky), F (Fine) and D (High Clouds) are assumed as rain free and the hourly rainfall for the raining cases (Type A, B and C) are

calculated from fractional coverage (FC) of clouds with cloud top colder than a certain threshold temperature in the area by applying linear relations shown in Table 1. The threshold temperatures and proportional contants shown in Table 1 were determined by calculating the linear regression between area-averaged rainfall and cold cloud fractional coverage from GMS IR data. Estimation of rainfall for a longer period is made by accumulating the hourly estimation for the period.

3. Data

The GMS IR imagery data and radar-AMeDAS composite rainfall data of the First Algorithm Intercomparison Program (AIP-1) data set of GPCP (Global Precipitation Climate Project) are used in the present study. The data area extends from 120°E - 147.5°E, 22.5°N-46.25°N, as shown in Fig.1, and the data period covers for a month from 1 to 30 June, 1989. The precipitation in this period over the area is mainly from Baiu front and a tropical depression.

As the method described in Xie[6] and Xie[7] was originally developed for areas of about 10^4 km^2 over the main islands of Japan, the entire area of AIP/1 as shown in Fig.1 is divided into 22×19 meshes of 1.25° latitudes × 1.25° longitudes and rainfall is estimated for each mesh.

The data set includes 720 hourly GMS IR observations in the 30 day period, from 00Z 1 to 23Z 30 June, 1989. The original GMS VISSR IR data have been interploted into a form that each pixel has a spatial resolution of 0.05° latitude×0.065° longitude. So the total IR pixel number in each mesh is 500. IR data at each pixel is in a digital form ranging from 0 to 255, which can be converted into equivalent blackbody temperature, T_{BB} by referring the calibration table in the data file. In order to estimate total cloud amount and to discriminate cloud type, T_{BB} histograms are constructed and the 4 IR cloud feature parameters (see Table 3 in Xie[6]) are calculated for every mesh.

The data set of Radar-AMeDAS rainfall is used as the ground truth of rainfall in the present study, which includes 720 houly rainfall distributions obtained by raingages of AMeDAS network supplemented by weather radar

observation (Takemura[8]) for the period. The network constituting of 22 weather radars and about 1300 AMeDAS raingages supplies a reliable ground truth of rainfall over and near the main islands of Japan. The rainfall data used here have the same spatial resolution as that of the IR data. Here in this study, the areal-averaged rainfall in each mesh of 1.25° latitudes × 1.25° longitudes are calculated and employed as the ground truth of rainfall.

4. Extension of the Estimation Method

Among the whole procedures of rainfall estimation described in section 2, discrimination of cloud type and derivation of rainfall may be most critical to geographic changes. For this reason, the method of discrimination of cloud type is first tested with the present data set. The results showed a high correct ratio of about 70% when compared with the concurrent subjective cloud type composed by the Meteorological Satellite Center of Japan meteorological agency (JMA) for several meshes in the area. This correct ratio may be enough for applying the original method to the whole area.

The necessary parameters in the estimation of the rainfall are the threshold temperatures and proportional contants as shown in Table 1. A preliminary study showed, however, that the threshold temperatures to define cold cloud fractional coverage FC do not vary so much within the present data area . So, the cloud type discrimination method and the threshold temperatures are thus decided to be kept as the same as those in the previous studies as summarized in section 2 (Xie[6)7)]), and the recalculation of the proportional constants between hourly rainfall and FC are made for the 3 raining types of clouds.

Although the proportional contants can be affected by many meteorological factors such as air temperatures, instability and amount of water vapor, the constants are assumed simply to be depent upon the latitudes in the present latitudes. Proportional contants between hourly rainfall and FC are thus calculated for various latitudes by using the IR and radar-AMeDAS rainfall data in the meshes with at least 5 gage observations. Fig.2a,b and c show the

results for the clouds of type A, B and C, respectively. The proportional contants tend to increase linearly from north to south, in general, for all of the three cloud types.

Based upon the results shown in this figture, the proportional contants are then taken as the linear functions of latitude, and the related parameters are determined from the data shown in Fig.2 by making linear regression for the three raining types of clouds, whose results are shown in Table 2. The slope for the proportional contant of type B (cumulonimbus) is 0.106, which is nearly twice as large as those of type A (cumulus) and C (middle cloud). This means that the development of cumulonimbus is most sensible to the latitude, which may comes from changes in air temperature and water vapor with latitude.

So, in the present study, rainfall estimation is made from cold cloud fractional coverage FC for each mesh by applying proportional constants shown in Table 2, which is the functions of the latitude.

5. Application of the Extended Method

The extended method described in the previous section is then applied to estimate rainfall for the entire area and period and the results are compared with the concurrent radar-AMeDAS composite rainfall for meshes over Japanese islands.

The appendix shows the distributions of estimated daily rainfall for entire area (middle) and observed daily rainfall over Japanese islands (left), together with surface weather charts at 0900JST (right) for the period from 1 to 30 June, 1989. The rainfall has been plotted in 8 classes, that is, non-rain; R<1 mm; R<2 mm; R<5mm; R<10mm; R<20mm; R<50mm and R>=50mm. The figures plotted above weather charts is the mean and maximum estimation errors in the meshes with at least 5 gages over Japanese islands for the day. The Baiu front is located over the main islands of Japan and their adjacent ocean during this period. Lows originated over the China Continent moved eastward along the front and brought rainfall over the area. A tropical depression also entered into this area from south, landed on Kyushu island and resulted in rainfall in the period from 23 to 25 of June.

Table 3 shows the statistical comparison between the estimation and the radar-AMeDAS rainfall over Japanese islands for 1, 3, 6, 12, 24 hours and 2, 5, 10, 30 days. The correlation increased from 0.41 for 1 hour to 0.88 for 30 days, while the relative error, defined as the ratio of mean absolute error to the mean of the radar-AMeDAS rainfall, descreased from 107% for 1 hour to 17% for 30 days. The accuracy of the estimation shown here satisfies the useful level of the requirement for climatic study presented by Browning[9], that is

100% and 20% for the 6 hour and the monthly rainfall.

Fig. 3 shows the scatter plot of the estimation and radar-AMeDAS data of daily rainfall. The estimation tends to overestimate in the light rain case and to underestimate in the heavy rain case. There is an obvious upper limit for estimating heavy rainfall, because a linear relation between rainfall and cold cloud fractional coverage (FC) is adpoted and FC is less than unity in the present method.

Fig. 4 shows the same scatter plot for 30 day rainfall. When compared with that for 24 hours as shown in Fig. 3, the agreement between estimation and radar-AMeDAS rainfall is improved greatly, especially for the cases with rainfall smaller than 400 mm/month. However, underestimation still extists for cases with rainfall larger than 400 mm/month.

The spatial distribution patterns of the estimation and the radar-AMeDAS rainfall are also compared for 24 hour and 30 day. As shown in the Appendix, the estimated daily rainfall distributions agree relatively well with those of radar-AMeDAS rainfall in general. However, overestimation for light rain and underestimation for heavy rain are found systematicaly in the edge and central parts of a disturbance, respectively. This is considered to be resulted from the difference in relationship between rainfall and cloud coverage in various parts of a disturbance. The cloud top varies little from the central to the edge parts, while the ascending current and rainfall concentrate mainly in the central part. As the result, the present method tends to overestimate the rainfall in the edge of disturbances and to underestimate the maximum of the rainfall in the central part.

The estimation error is found to be also resulted in from the assumption of rain-free in cases with cloud amount less than 0.7 (Type S,F) and from mis-discrimination of the cloud type. Table 4 shows rainfall in the cases the cloud type is determined as the non-rain three types of clouds from IR data. Among whole 12268 cases of type S and F, which are estimated as non-rain in the present method, 2864 cases (23%) are rainy with rainfall larger than 0.0 mm. Among 2801 cases of type D (Cirrus), which are discriminated also as non-rain, 1532 cases (54.7%) are rainy and 324 cases (11.6%) with rainfall larger than 1.0 mm/hr. This should be decreased in the future development of the method. In cases with cloud type of A (Cumulus), B (Cumulonimbus) and C (Middle Clouds), the warm cloud case with the fractional coverage (FC) of zero also results in rainfall estimation of 0.0 mm. Table 5 shows the statistics of real rainfall in such cases which are estimated as non-rain in cloud type A,B and C. About 44% of such cases are truly non-rain but 56% are rainy. This error in estimation is considered to be caused in the mis-discrimination of cloud type and in the adpotion of a temperature threshold.

Geographical distribution of relative error for 24 hour rainfall estimation is shown in Fig.5. The larger error seems to appear in the mountaineous areas. This is considered to be resulted from differences in the relation between rainfall and cloud coverage in mountaineous areas from that in the plain areas.

The agreement in spatial ditributions between estimation and radar-AMeDAS rainfall is then investigated for longer period. Fig.6a and b show the total estimation and radar-AMeDAS rainfall distributions for 30 days period. The

rainfall band extends from east to west over Japan and its adjacent ocean has been estimated well, but heavy rainfall larger than 500 mm in Fig.5a have been underestimated.

Comparison of time changes of the estimation and radar-AMeDAS rainfall is also made for all meshes with at least 5 gages over Japanese islands. Fig.7a,b show examples of the time series at mesh (35.00°N - 36.25°N; 133.75°E - 135.00°E) for 3 and 24 hour rainfall. The rainfall in this mesh during the period from 1 to 30 June, 1989 is characterized by five peaks on 5th, 9th, 16th, 23rd and 28th June, among which four peaks are due to passages of lows along the Baiu front and the other one is due to the landing of a tropical depression.

In the time series of 3 hour rainfall, the estimation reproduces the main peaks of the radar-AMeDAS rainfall, however, the magnitude of the rainfall is underestimated greatly in general. The correlation between the estimation and radar-AMeDAS rainfall is 0.467 and the mean absolute error is 1.7 mm, which is about 105 % of the mean of the radar-AMeDAS rainfall in the mesh.

For 24 hr rainfall, the correlation between the estimation and the radar-AMeDAS rainfall is 0.552 and the mean absolute error is 10.5 mm, which is about 81% of the mean of the rainfall. As shown above, the agreement between the time change pattern has been improved for the 24 hour rainfall.

6. Conclusion

The rainfall estimation method developed for the limited area over Japanese islands (Xie[7]) is extended to estimate the rainfall for wider area surrounding Japan, using the GMS IR imagery data and radar-AMeDAS composite rainfall data in June 1989.

After investigating the relationship between rainfall and cloud over Japanese islands, threshold temperatures to define cold cloud fractional coverage FC for the three raining types of clouds (A:cumulus; B:cumulonimbus and C:middle cloud) are determined to be kept the same as those used in the previous study (Xie[7]). The proportional contants to calculate hourly rainfall from FC are then taken as linear functions of latitudes and determined for the three types of clouds.

The extended method provides a relatively good estimation for meshes of 1.25° latitudes × 1.24° longitudes, when compared with the concurrent rainfall obtained from radar-AMeDAS network over Japan. The correlations and relative errors are 0.595 and 96% for daily rainfall and 0.88 and 17% for monthly rainfall, which satisfy the useful level of the rainfall data to be used in a climatic study. However, the estimation data tends to underestimate some heavy rainfall peaks and overestimate in light rain cases, especially for shorter estimate periods.

The spatial distribution of estimated rainfall agrees relatively well with that of observed rainfall. The main errors are the underestimation in the center and the overestimation in the edge of a rain area. The time changes of

the estimation catch the main peaks in the observation, but the peak values are underestimated greatly in shorter estimate periods.

The estimation errors may also come from the ignorance of the rainfall in the meshes with cloud amount smaller than 0.7 and also from the adpotion of a simple linear equation to relate hourly rainfall with the cold cloud fractional coverage FC. These points should be improved in the further study.

Acknowledgements

The author would like to thank Prof. Y. Mitsuta of the Disaster Prevention Research Institute (DPRI) of Kyoto University for his continous guidances and encouragements during the study. The author is also grateful to Dr. P. A. Arkin and Dr. J. E. Janowiak of NMC/NOAA, for supplying the satellite and ground data of AIP/1 and commenting on the manuscript of the paper. Discussions with Prof. M. Yamada and other members in the Severe Storm Division of DPRI were very helpful. The computations were performed by FACOM M-730 computer at the Information Processing Center of DPRI.

References

1) Barrett, E.T., and D.W. Martin: The use of satellite data in rainfall monitoring. Academic Press, 1982, pp.340.

2) Arkin P.A., and P.E. Ardanuy: Estimating climatic-scale precipitation from space: a review. J.Climate, Vol.2, 1989, pp.1229-1238.

3) Griffith, C.G., W.L. Woodley, P.G. Grube, D.W. Martin, J. Stout and D.N. Sikdar: Rain estimation from geosyschronous satellite imagery-visible and infrared studies. Mon. Wea. Rev., Vol.106, 1978, pp.1153-1171.

4) Arkin P.A., and B.N. Meisner: The relationship between large-scale convective rainfall and cloud cover over the western hemisphere during 1982-84. Mon. Wea. Rev., Vol.115, 1987, pp.51-74.

5) Xie P., and Y. Mitsuta: Rainfall estimation from GMS infrared and visible imagery data. Annuals. Disas. Prev. Res. Inst., Kyoto Univ., Vol.31B-1, 1988, pp.201-217.(in Japanese)

6) Xie P.: Nephanalysis of the GMS imagery data. Bull. Disas. Prev. Res. Inst., Kyoto Univ., Vol.40, 1990, pp.57-77.

7) Xie P.: Rainfall estimation in the midlatitudes from GMS infrared imagery data. Bull. Disas. Prev. Res. Inst., Kyoto Univ., Vol.41, 1991, pp.109-120.

8) Takemura, Y.,: Application of the digital weather dradar. Weather, Vol.27, pp.7402-7405. (in Japanese)

9) Browning, K.A.: Rain, rainclouds and climate. Q.J.R.Meteorol.Soc., Vol.116, 1990, pp.1025-1051.

Caption

Table 1 Thresholds and Regressional Equations Used in Xie[7]

E_1: IR estimation of hourly rainfall in mm

FC: cold cloud fractional coverage

Table 2 Thresholds and Regressional Equations Used in the Extended Method

El: IR estimation of hourly rainfall in mm

ϕ: latitude in degree

FC: cold cloud fractional coverage

Table 3 Comparison between Radar-AMeDAS composite rainfall and IR Estimation of Raifnall

OBS. : mean of the radar-AMeDAS composite rainfall

EST. : maen of the IR estimation

RATIO : ratio of EST. to OBS.

CORR : correlation coefficient between the estimation and the composite rainfall

BIAS : bias of the estimation compared to the composite rainfall

R.E. : relative error defined as the rastio of BIAS to OBS.

Table 4 The Observed Rainfall for the Case of Non-Rain Cloud Type, S (Clear Sky), F (Fine) and D (Cirrus).

Table 5 Classification of the Rainfall for the Cloud Type of A (Cumulus), B (Cumulonimbus) and C (Middle Clouds) with Estimated Rainfall of 0.0mm.

Fig. 1 The investigation area of GPCP-AIP/1.

Fig. 2 Proportional constants at various latitudes for the 3 raining types of clouds.

Fig. 3 Scatters of the radar-AMeDAS composite rainfall and IR estimation of rainfall for 24 hour.

Fig. 4 Same as Fig.3, except for 30 day.

Fig. 5 Distribution of relative error for 24 hour estimation.

Fig. 6 Distributions of a) radar-AMeDAS composite rainfall and b) IR estimation of rainfall of June 1989 over the investigation area of GPCP-AIP/1.

Fig. 7 Time series of radar-AMeDAS composite rainfall (dashed line) and IR estimation of rainfall (thin line) at grid (35.00°-36.25°N; 133.75°-135.00°E) for a) 3 hour and b) 24 hour accumulated data.

Appendix The distributions of estimated daily rainfall for the entire area (middle), observed daily rainfall over Japanese islands (left) and the surface weather charts at 0900JST (right) for the period from 1 to 30 June, 1989. The rainfall has been plotted into 8 classes: non-rain; $R < 1$ mm; 1 mm $\leqq R <$ 2 mm; 2 mm $\leqq R <$ 5 mm; 5 mm $\leqq R <$ 10 mm; 10 mm $\leqq R <$ 20 mm; 20 mm $\leqq R <$ 50 mm and $R \geqq$ 50 mm.

Table 1

Thresholds and Regressional Equations

Used in Xie[7)]

TYPE	THRESHOLD	REGRESSIONAL EQUATIONS
A	245 K	$E_I = 2.527 \cdot FC_A$
B	235 K	$E_I = 2.820 \cdot FC_B$
C	255 K	$E_I = 1.238 \cdot FC_C$

E_I: IR estimation of hourly rainfall in mm

FC: cold cloud fractional coverage

Table 2

Thresholds and Regressional Equations

Used in the Extended Method

TYPE	THRESHOLD	REGRESSIONAL EQUATIONS
A	245 K	$E_I = (4.779 - 0.059\phi)FC_A$
B	235 K	$E_I = (6.383 - 0.106\phi)FC_B$
C	255 K	$E_I = (3.956 - 0.062\phi)FC_C$

E_I: IR estimation of hourly rainfall in mm

ϕ : latitude in degree

FC: cold cloud fractional coverage

Table 3

Comparison between Radar-AMeDAS Composite Rainfall and IR Estimation of Rainfall

DURATION	OBS.	EST.	RATIO	CORR.	BIAS	R.E.
1 HR	0.4 mm	0.4 mm	0.98	0.41	0.5 mm	107.2%
3 HR	1.3	1.3	0.98	0.45	1.3	98.1
6 HR	2.6	2.6	0.98	0.48	2.4	91.6
12 HR	5.3	5.2	0.98	0.54	4.3	82.0
24 HR	10.3	10.2	0.99	0.59	7.5	73.1
2 DAY	21.3	20.7	0.97	0.61	13.1	61.6
5 DAY	53.2	51.2	0.96	0.74	18.0	33.8
10 DAY	93.1	91.9	0.99	0.81	25.6	27.5
30 DAY	279.4	275.6	0.99	0.88	48.1	17.2

OBS. : mean of the radar-AMeDAS composite rainfall

EST. : maen of the IR estimation of rainfall

RATIO : ratio of EST. to OBS.

CORR : correlation coefficient between the estimation of rainfall and the composite rainfall

BIAS : bias of the IR estimation compared to the composite rainfall

R.E. : relative error defined as the rastio of BIAS to OBS.

Table 4

The Observed Rainfall for the Case

of Non-rain Cloud Types, S (Clear Sky), F (Fine) and D (Cirrus)

OBSERVED RAINFALL	CLOUD TYPE			
	S	F	D	TOTAL
NON-RAIN	6717	2687	269	10673
R=0 mm	83.2%	64.1%	45.3%	70.8%
LIGHT RAIN	1340	1427	1208	3975
R<1 mm	16.6%	34.0%	43.1%	26.4%
MODERATE RAIN	17	80	297	394
R<5 mm	0.2%	1.9%	10.6%	2.6%
HEAVY RAIN	0	0	27	27
R>=5 mm	0%	0%	1.0%	0.2%
TOTAL	8074	4194	2801	15609

Table 5

Classification of the Rainfall

for the Cloud Type of A (Cumulus), B (Cumulonimbus) and C (Middle Clouds)

with Rainfall Estimation of 0.0 mm

OBSERVED RAINFALL	CLOUD TYPE			
	A	B	C	TOTAL
NON-RAIN	168	450	549	1167
R=0 mm	56.6%	45.4%	40.4%	44.1%
LIGHT RAIN	118	477	768	1363
R<1 mm	39.7%	48.1%	56.4%	51.4%
MODERATE RAIN	11	65	44	120
R<5 mm	3.7%	6.5%	3.2%	4.5%
HEAVY RAIN	0	0	0	0
R>=5 mm	0%	0%	0%	0%
TOTAL	297	992	1361	2650

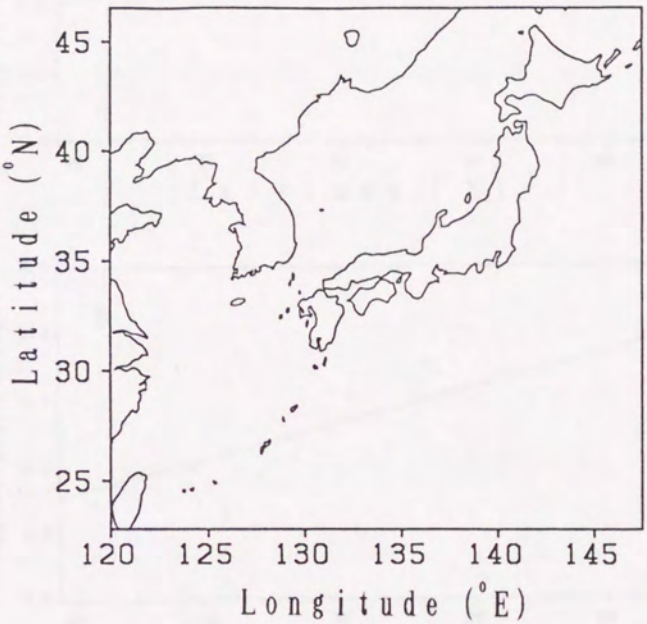

Fig. 1

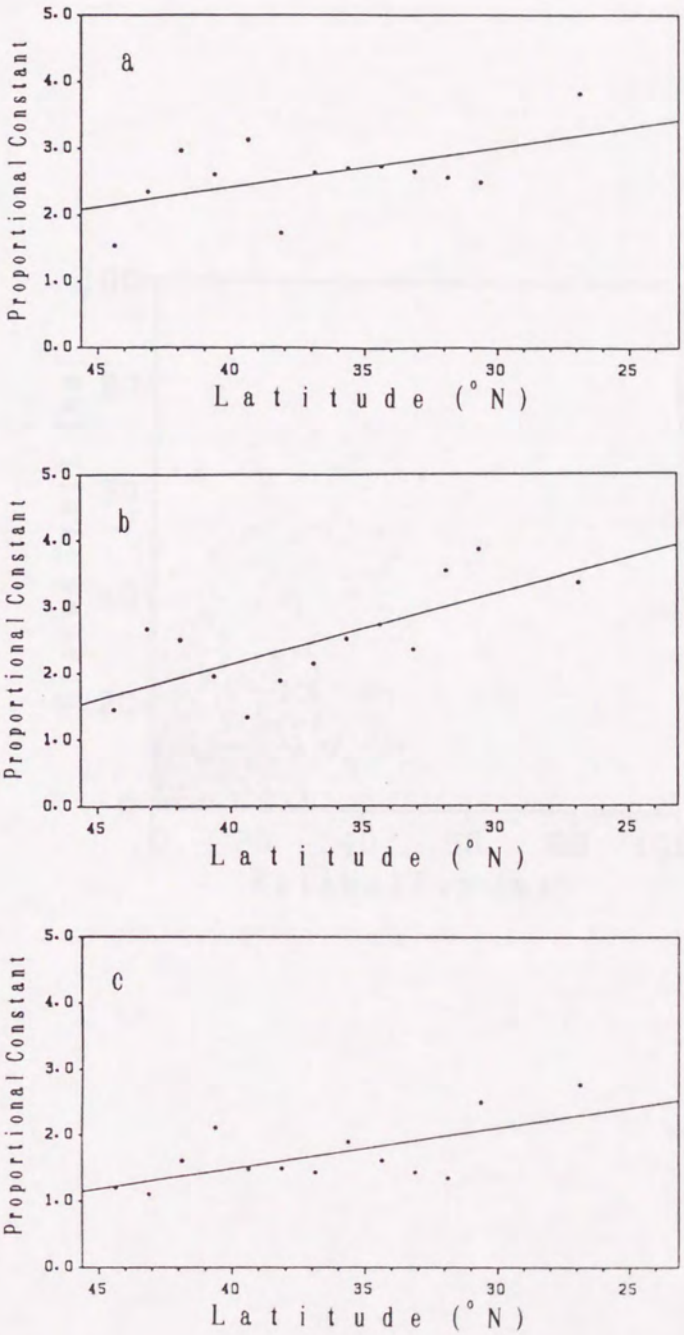
a
b
c
Proportional Constant
5.0
4.0
3.0
2.0
1.0
0.0
45
40
35
30
25
Latitude (°N)

Fig. 2

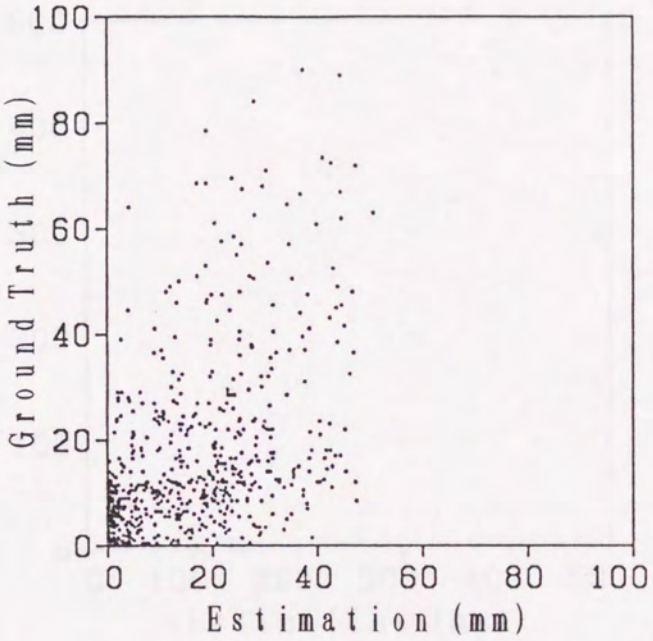

Fig. 3

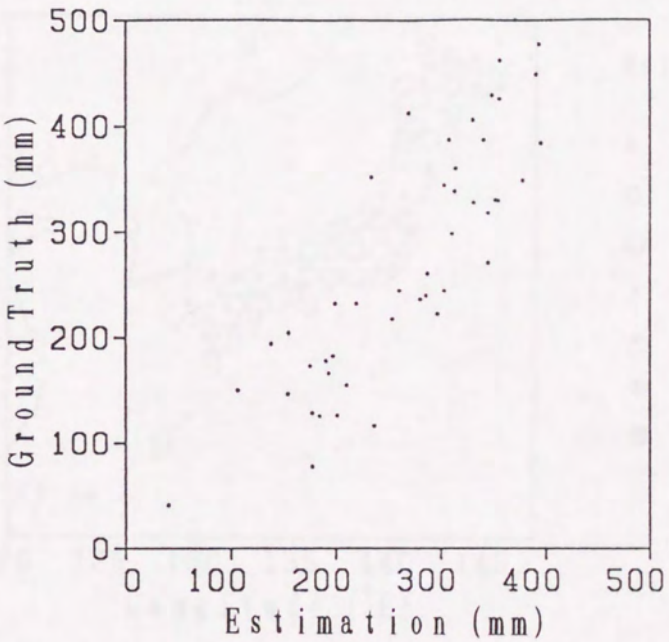
500
400
300
200
100
0
Ground Truth (mm)
0
100
200
300
400
500
Estimation (mm)

Fig. 4

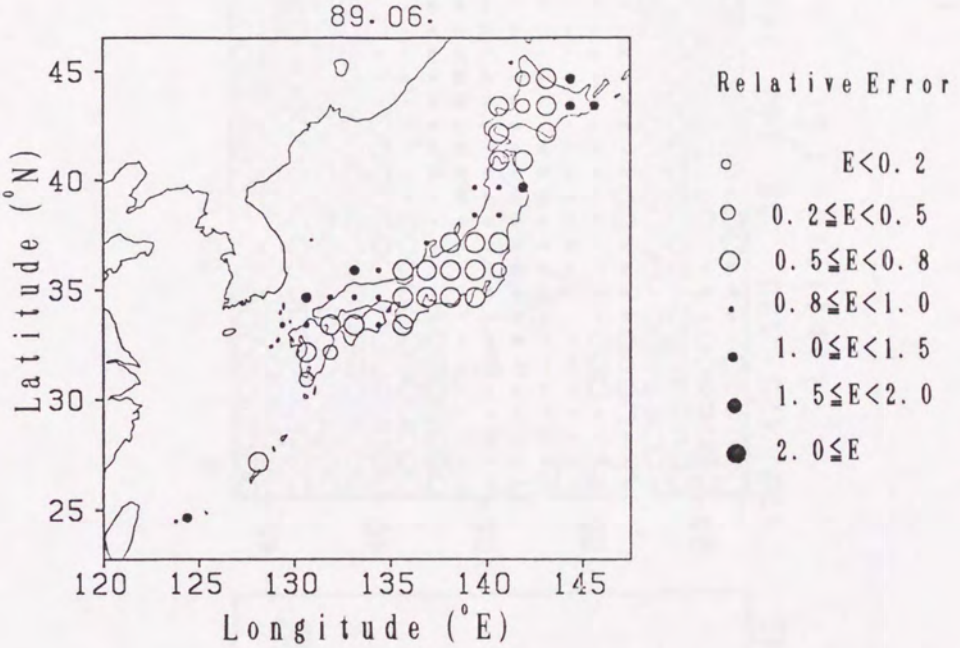
89.06.
45
40
35
30
25
Latitude (°N)
120
125
130
135
140
145
Longitude (°E)
Relative Error
E<0.2
0.2≦E<0.5
0.5≦E<0.8
0.8≦E<1.0
1.0≦E<1.5
1.5≦E<2.0
2.0≦E

Fig. 5

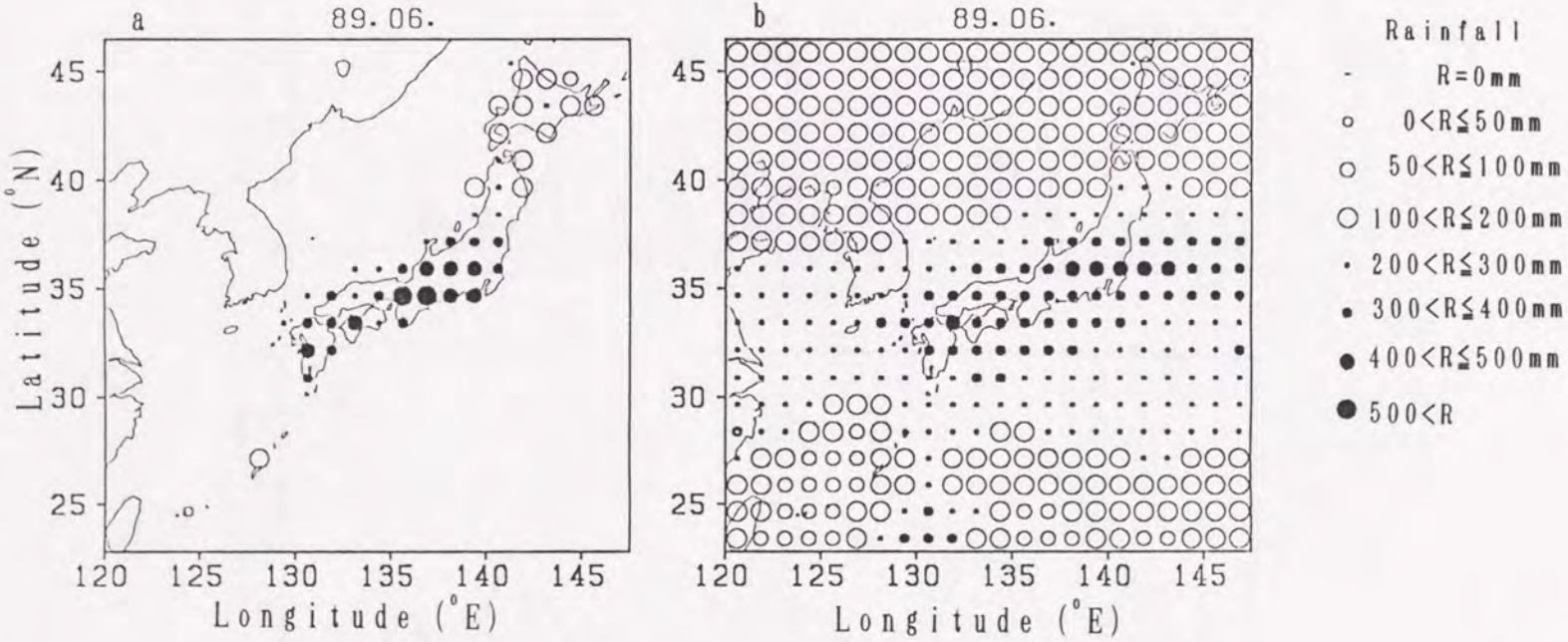
a
89.06.
b
89.06.
Latitude (°N)
Longitude (°E)
Rainfall
R=0mm
0<R≦50mm
50<R≦100mm
100<R≦200mm
200<R≦300mm
300<R≦400mm
400<R≦500mm
500<R

Fig. 6

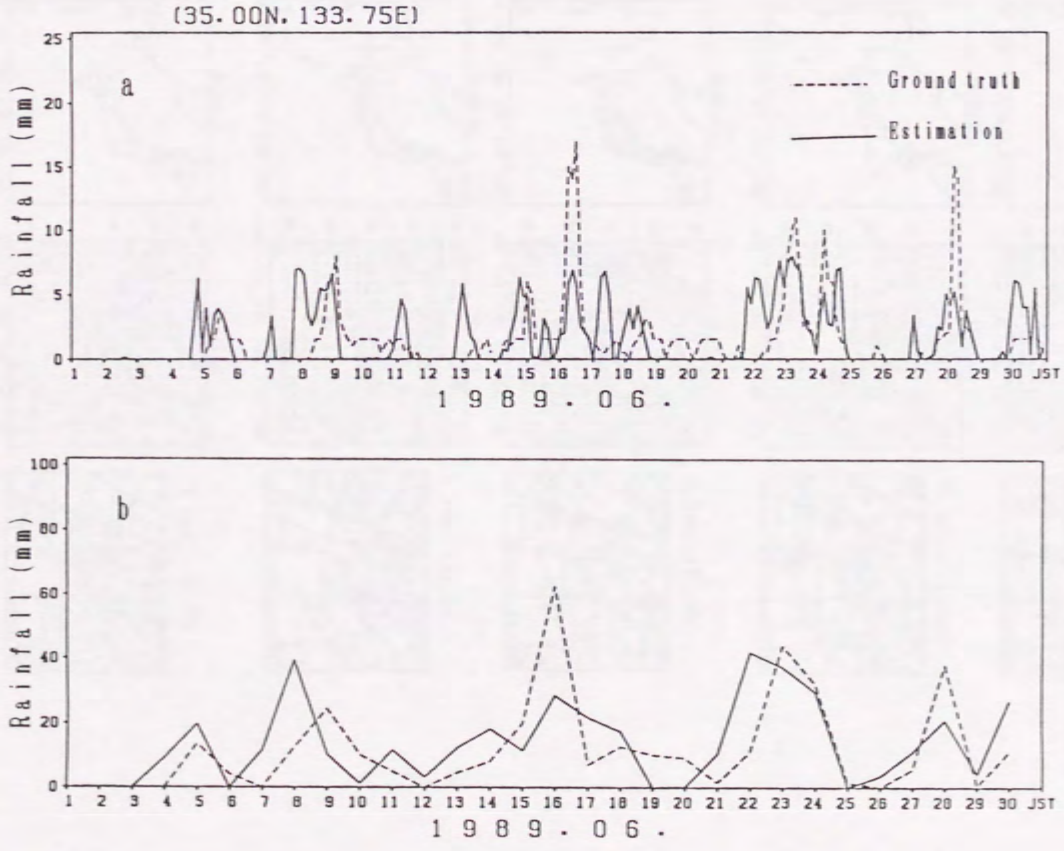
(35.00N, 133.75E)
a
Ground truth
Estimation
Rainfall (mm)
1989.06.
b
Rainfall (mm)
1989.06.

Fig. 7

Appendix

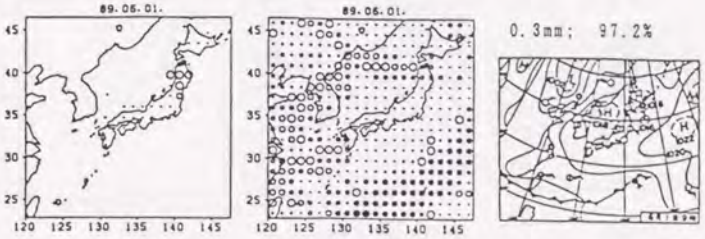
89.06.01.
89.06.01.
0.3mm; 97.2%

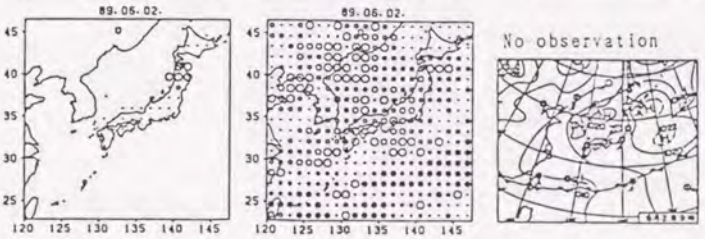
89.06.02.
89.06.02.
No observation

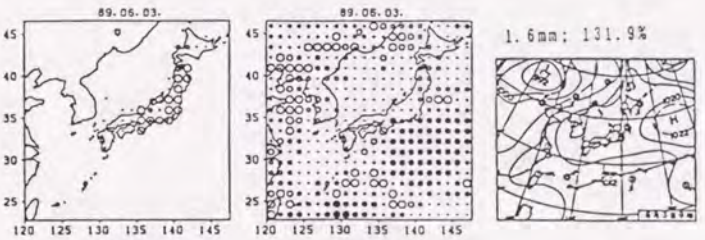
89.06.03.
89.06.03.
1.6mm; 131.9%

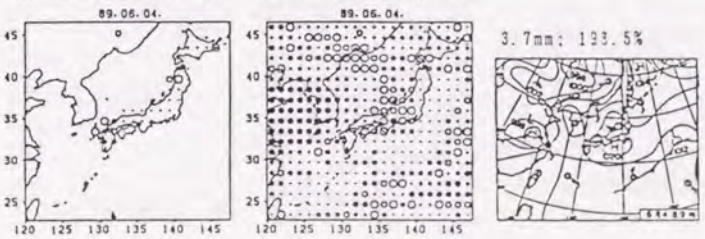
89.06.04.
89.06.04.
3.7mm; 193.5%

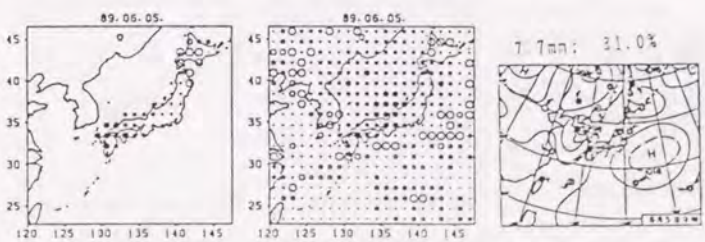
89.06.05.
89.06.05.
7.7mm; 31.0%

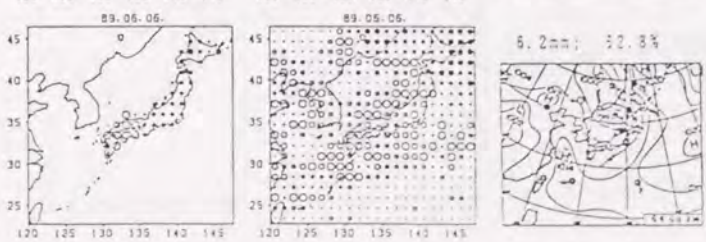
89.06.06.
89.06.06.
6.2mm; 92.8%

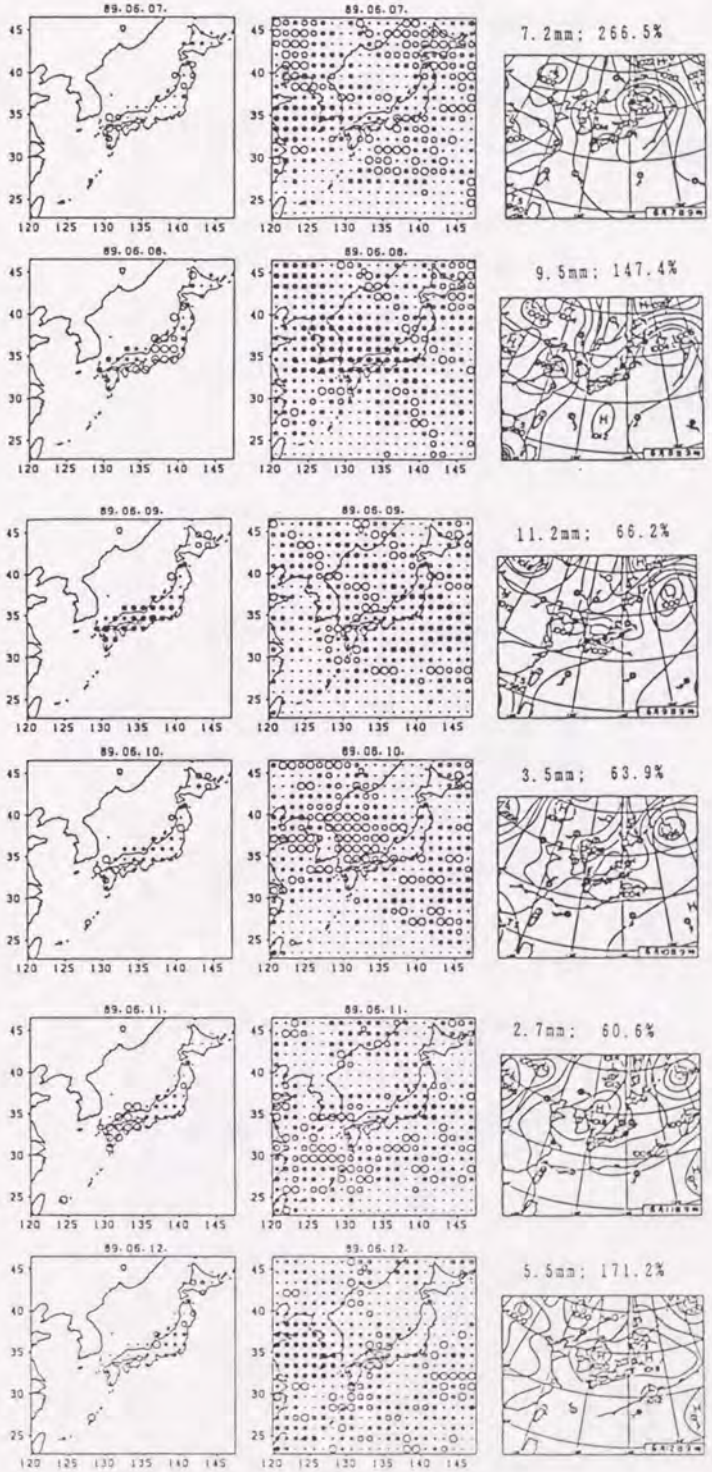
89.06.07.
89.06.07.
7.2mm; 266.5%
89.06.08.
89.06.08.
9.5mm; 147.4%
89.06.09.
89.06.09.
11.2mm; 66.2%
89.06.10.
89.06.10.
3.5mm; 63.9%
89.06.11.
89.06.11.
2.7mm; 60.6%
89.06.12.
89.06.12.
5.5mm; 171.2%

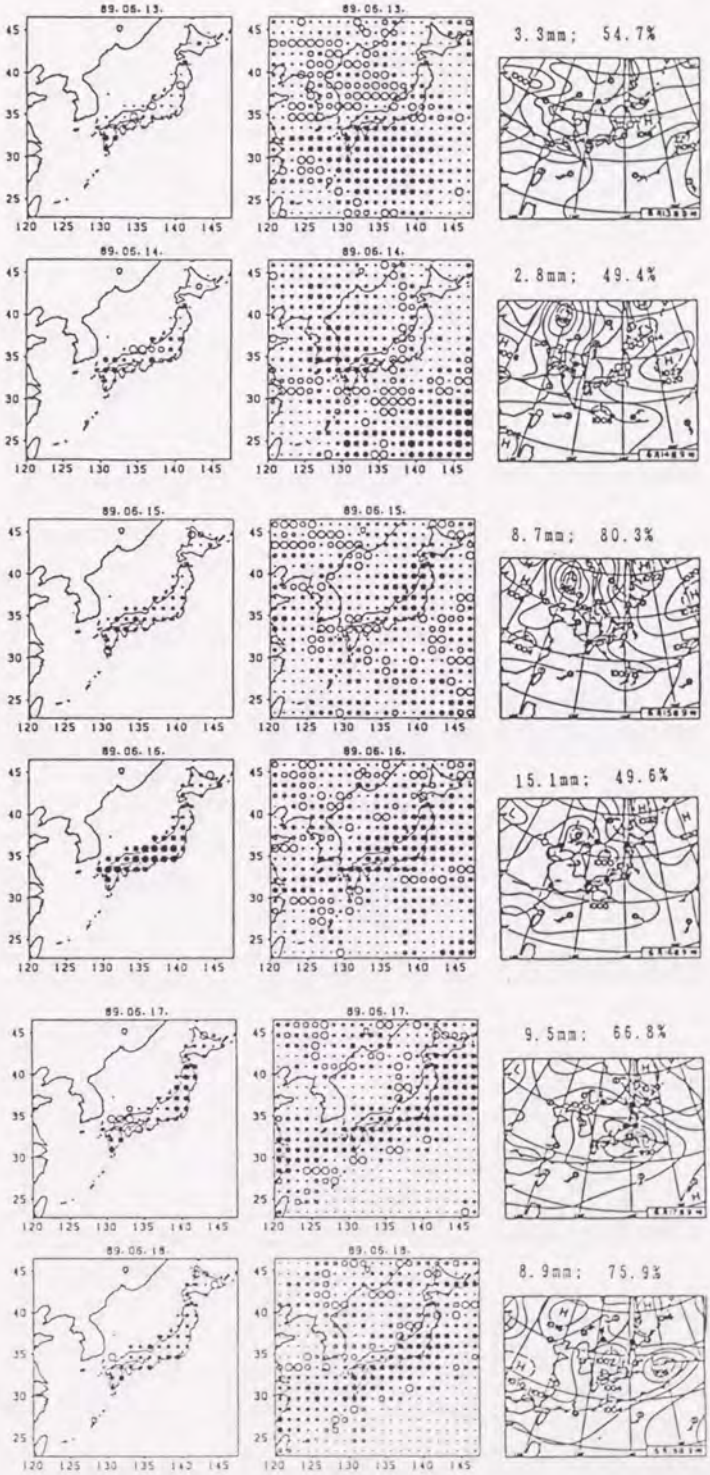
89.06.13.
89.06.13.
3.3mm; 54.7%
89.06.14.
89.06.14.
2.8mm; 49.4%
89.06.15.
89.06.15.
8.7mm; 80.3%
89.06.16.
89.06.16.
15.1mm; 49.6%
89.06.17.
89.06.17.
9.5mm; 66.8%
89.06.18.
89.06.18.
8.9mm; 75.9%

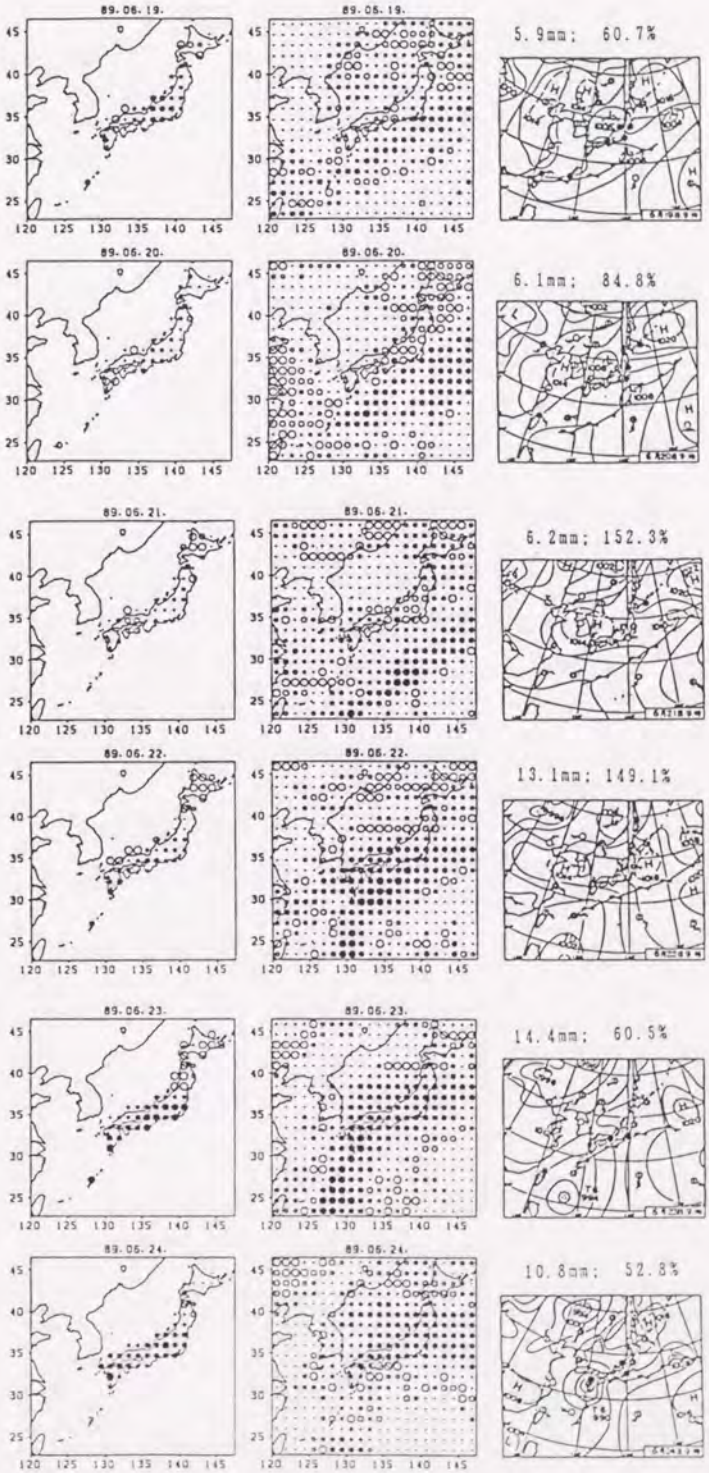
89.06.19.
89.06.19.
5.9mm; 60.7%
89.06.20.
89.06.20.
6.1mm; 84.8%
89.06.21.
89.06.21.
6.2mm; 152.3%
89.06.22.
89.06.22.
13.1mm; 149.1%
89.06.23.
89.06.23.
14.4mm; 60.5%
89.06.24.
89.06.24.
10.8mm; 52.8%

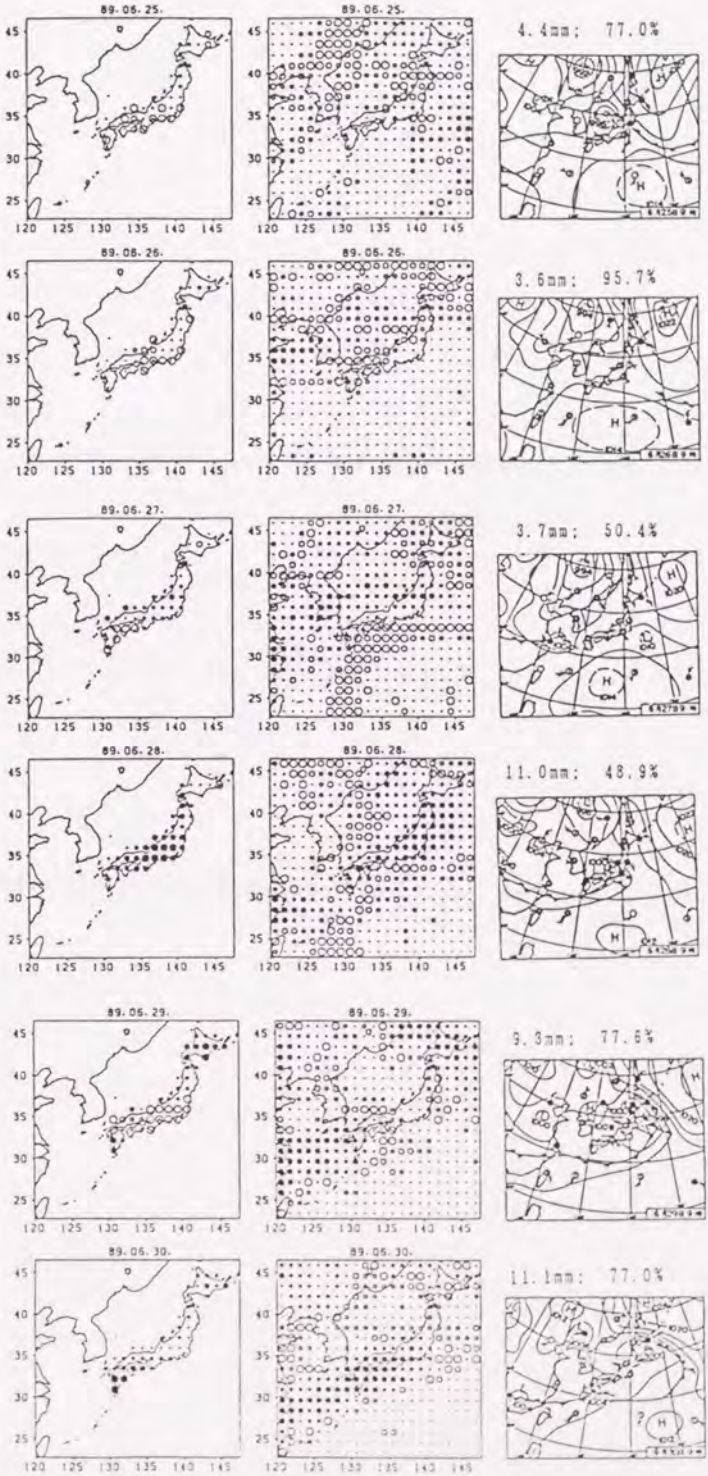
89.06.25.
89.06.25.
4.4mm; 77.0%
89.06.26.
89.06.26.
3.6mm; 95.7%
89.06.27.
89.06.27.
3.7mm; 50.4%
89.06.28.
89.06.28.
11.0mm; 48.9%
89.06.29.
89.06.29.
9.3mm; 77.6%
89.06.30.
89.06.30.
11.1mm; 77.0%

Comparisons of Rainfall on the Japanese Islands and Their Adjacent Ocean

by Pingping Xie

Submitted to Bull. Disas. Prev. Res. Inst., Kyoto Univ.

Abstract

Rainfall features of the Baiu season estimated from GMS IR images are investigated on the Japanese islands and their adjacent ocean for June 1989. The total monthly rainfall for the period is distributed in a band-like shape extending from west to east, showing its maximum on 35°N in the latitudinal section and a sudden decrease to the west of 130°E in the longitudinal section. The latitudinal distributions of rainfall relative to the Baiu front show almost the same shape with their maximum at 1.25° north of the front at the surface over both land and ocean, but the peak amount is larger over the island than that over the ocean. The temporal changes of rainfall are dominated by a period of synoptic scale for all regions over both land and ocean, and secondly peak corresponding to daily variation is observed only over the continent. The rainfall region moves eastward along the Baiu front with almost same phase speed of about 7.5° longitudes per 12 hours over almost all regions.

1. Introduction

Investigation of the spatial distribution and temporal change of rainfall of the Baiu front (Mei-yu in China) is an important subject in understanding the water and energy budget in the East Asia. The Baiu front extends widely from the central portion of China to the east of Japan, moves slowly from south to north during the period from late spring to summer.

Yoshino[1] investigated the climatic rainfall characteristics of Baiu front by using rain gage data of 1954 and showed a band-like distribution of rainfall over China continent and Japanese islands (Fig.1). The distribution over the East China sea was unknown, but he tried to link the isohyets subjectively between the east coast of China and the Kyushu island. During the last two decades, series works of Ninomiya, Akiyama and their collabotators (e.g. Ninomiya and Akiyama[2)3)], Akiyama[4)5)], Ninomiya and Muraki[6)], Ninomiya and Mizuno[7)], Akiyama[8)9)10)]) have contributed much on understanding of the features of Baiu rainfall by using mainly radar and gage observations. Their works have revealed many important aspects of the nature of the clouds and rainfall of the Baiu front. The main conclusions are that 1) frontal depressions with meso-α scale develop along the Baiu front; 2) intense Baiu rainfall is produced by successive development of these depressions; and 3) in many cases, precipitation system is composed of a few meso-β precipitation systems. However, their studies have also been limitted to the clouds and rainfall over land (mainly over Japanese islands) because of lack of data over the ocean. Rainfall features of the Baiu front have not been investigated neither over the East China sea nor over the Pacific ocean and the Japan sea, because of shortage of the observational data. In order to

investigate the rainfall features of the Baiu front as a whole system, the rainfall data with an adequate accuracy is necessary over ocean.

The practical use of satellite observation has made it possible to infer rainfall over both land and ocean especially for those in the tropical areas where convective clouds dominate (e.g. Arkin[11], Arkin and Meisner[12], Shin et al.[13], Janowiak and Arkin[14]. Estimation of rainfall in midlatitudes, however, has been a much more difficult task because of the existence of non-raining cirrus and raining stratiform clouds (Wylie[15], Xie and Mitsuta[16]). Recently, the present author has developed a method to estimate rainfall in midlatitudes from the IR observation data of the Geostationay Meteorological Satellite of Japan (GMS) (Xie[17][18]). The method has shown a resonable success in estimating rainfall of the Baiu front in June 1989 (Xie[19]).

The present paper will give a description and analysis of the features of rainfall of the Baiu front as the first step toward the understanding of the Baiu front as a system, by using the results of the previous research on the estimation of rainfall in 1.25° meshes (Xie[19]). Among the many aspects of rainfall, the present work will be focused on 1) spatial distribution of the rainfall of Baiu front in a climatic scale; 2) temporal change features of rainfall at various regions over land and ocean; 3) phase speed of rainfall region along the Baiu front.

2. Data

The data set of the First Alrogithm Intercomparison Program of Global Precipitation Climatogy Project (GPCP-AIP/1) is used in the present study to investigate the rainfall features of Baiu front. The data area extends from 120°E - 147.5°E; 22.5°N - 46.25°N and the period covers from 1 to 30 June, 1989 (see Fig.1 in Xie[19]).

The hourly rainfall has been estimated for 22×19 meshes with size of 1.25° ×1.25° in latitude and longitude for the entire period from the hourly observation of GMS IR images, by using the modified rainfall estimation method described in Xie[19]. This estimation has been shown to satisfy the useful level of accuracy requirement for climatic application presented by Browning[20], when compared with the results of the concurrent radar-AMeDAS composite rainfall over the main islands of Japan (Xie[19]). Besides the satellite data mentioned above, daily surface weather charts on 0900JST for the period are also employed to determine the positions of Baiu front. These position data are then used to derive latitudinal distribution of rainfall relative to the Baiu front.

During the period, a large band of cloud and rainfall moved slowly south and north. Several depressions developed and moved eastwardly along the front in intervals of about 7 days. As shown in the daily rainfall distributions of the period in the Appendix of Xie[19], these depressions resulted in rainfall over both land and ocean over the investigation area.

3. Spatial Distribution of Rainfall

Fig. 2 shows the distribution of the estimated monthly rainfall over the area, together with the estimated average cloud amount. Positions of the Baiu front obtained from the surface weather charts on 0900JST of each day for the whole period are also ploted on these figtures .

While the cloud amount forms a band extending from (120°E, 30°N) to (147.5°E, 35°N) almost continuously, the monthly rainfall distribution has a distinct break over the East China sea (120°E - 130°E). The band of the monthly rainfall larger than 300 mm centers on about 35°N and extends from 130°E to the east side of the area with width of about 5°N. Maximum with rainfall larger then 500mm is observed in the Kanto area. This result resembles well with the guess in the rainfall distribution over the East China sea by Yoshino [1] as shown in Fig. 1.

Fig. 3a and b show the averaged latitudinal and longitudinal profiles of rainfall (solid line) and cloud amount (dashed line) over the area for the whole period. The latitude profile (fig. 2a) of both rainfall and cloud amount shows a single peak shape extending from about 25 to 40°N. The rainfall peak of 325 mm appears at 35°N, and the peak of cloud amount of 0.63 is at 33.75°N, a little south to the rainfall peak in latitudinal profile.

In the longitudinal profile shown in Fig. 3b, both rainfall and cloud amount show nearly constant values (rainfall 210 - 230 mm, cloud amound 0.55 - 0.58) over areas to the east of 130°E (Kyushu), while those over the East China sea are obviously smaller than the values over land, with their minimum at

about middle of the East China sea. The decreases in rainfall and cloud amount are 14% and 34% when compared with those at Kyushu.

In order to investigate the rainfall features relative to the frontal structures over land and ocean, whole area east to 122.5°E (excluding portions over the east coast of China) is divided into 3×3 sub-regions as shown in Fig.4 and the latitudinal profiles of rainfall and cloud amount relative to the position of surface front are calculated by averaging the daily rainfall at various positions for the entire period of 30 days. Fig.5 shows the results for the 6 sub-regions with latitudes south of 41.25°N. No relative profile is obtained for the 3 sub-regions with latitudes north of 41.25°N, because the Baiu front did not move into the three sub-regions during the period.

The resultant relative profiles of rainfall and cloud amount have almost the same shapes for the whole 6 sub-gerions. The maximum of the rainfall is not just at the position of surface front, but about 1 mesh (1.25° latitudes) north to it. The values of rainfall and cloud amount, however, are different for the sub-regions over ocean and over land. Table 1 shows the rainfall (bottom) and cloud amount (upper) values at the peaks. The peak rainfall varies from 11 mm over the East China sea to 21 mm over the main islands of Japan, while the peak cloud amount varies from 0.71 to 0.85 for the same sub-regions. Both the rainfall and cloud amount have larger amount while the Baiu front lies over Japanese islands and smaller while over the surrounding ocean. The difference of rainfall peaks over the Japanese islands and their adjacent ocean is about 50%. These facts show that frontal rainfall peak is at the position where the slanting frontal surface gains higher altitude to north of the surface front and also that the rainfall pattern is of the same over the

islands and ocean but the peak amount of rainfall is larger over the islands than over the ocean by about 50%. Topography seems to account for this difference.

4. Temporal Change of the Rainfall

Temporal changes of rainfall are also investigated for the various subregions as shown in Fig.4. Fig.6 shows the power spectral density distributions of the area-averaged 3 hour rainfall for the subregions calculated by the Maximum Entropy Method (MEM). The data number of each time series is 240.

The spectra for the 9 subregions have well defined peaks at periods corresponding to the variations of synoptic scale (4 - 8 days). Another small peak is also seen at period of 1 day in the spectra of the subregion extending from 122.5°E - 130.0°E; 41.25°N - 46.25°N (Northeastern provinces of China). These facts suggest that the temporal changes of the area-averaged rainfall are dominated by the variations of synoptic scales for all of the 9 subregions, while that for the subregion over the China continent has an addtional peak related to the daily variation. This result is similar to the result for the spectra of high cloud amount of the Baiu front investigated by Akiyama[10], which shows obvious peaks in synoptic scale (about 5.86 days) over whole portions of the front and in daily scale only over the continent.

Fig.7 shows the spectum of the time series of the area averaged rainfall for the entire region to the east of 122.5°E. The spectra is characterized by two peaks at periods of about 7 days (synoptic) and 1 day (daily), respectively. The daily variation becomes distinct compared to those in the subregions caused by averaging in space.

5. Movement of the rainfall along the Baiu front

Fig. 8 shows the results of space-time correlations of rainfall when the Baiu front lies over various sub-regions shown in Fig. 4. 5 lines in each figture represent the correlations with lagged time of -12, -6, 0, 6 and 12 hours, respectively. Almost all of the correlation lines have single mode shapes, with their maximum at distance proportional to the time lag, suggesting the eastward movement of the rainfall region along the Baiu front with constant speed. The peak values of the correlations for time lag of ± 12 hours, however, are very low, which suggests that the rainfall pattern usally does not keeps its shape for period longer than 12 hours while moving eastward along the Baiu front. This fact agrees with the conclusions of Ninomiya and Akiyama[2)3)], in which they revealed that the rainfall of the Baiu front is directly caused from several meso scale cloud clusters.

Table 2 shows the phase speeds of the movement of the rainfall region for the 6 subregions which are determined from the correlations with time lag of ± 6 hours. The phase speeds are 7.5°E per 12 hours over most of the sub-regions except the sub-region over ocean to the south of Japanese islands, over which the speed is slower (5.0°E per 12 hours). The phase speed averaged over all of the sub-regions are 6.25°E per 12 hours or about 55 km/hr. This speed is almost the same as the wind speed at 500mb.

6. Conclusions

Rainfall features are investigated by using the satellite IR rainfall estimation data of June 1989 over an area of 27.5° longitudes × 23.75° latitudes surrounding Japan, with special attention on the spatial distribution, temporal change and the movement of the Baiu front.

The rainfall of the investigation period is mainly that of Baiu front, which moves slowly south and north. The accumulated monthly rainfall for the period has a band-like distribution, which extending from (120°E, 30°N) to (145°E, 35°N) with a width of about 5° latitudes. The latitudinal profile of the rainfall averaged from 120°E to 147.5°E shows that the rainfall of the Baiu front is in an one-mode shape with its peak at 35°N. The longitudinal profile of rainfall shows that the rainfall of the Baiu front has almost same values over longitudes east to Kyushu, but rainfall over the East China sea decreases to about 2/3 of that over Kyushu.

The latitudinal distribution of rainfall relative to the surface front also has an common one-mode shape, with its maximum at positions 1.25° north to the surface front. Although the shapes for the distributions are almost the same for all regions over both land and ocean, the peak amount over land (main islands of Japan) is about 1.5 times larger than that over ocean (the East China sea).

The temporal change of the rainfall is characterized by a dominant period of synoptic scale (about 7 days). The apprant daily variation of the rainfall is observed only over the Asian continent (Northeastern provinces of China).

The phase speeds of the eastward movement of rainfall along the Baiu front show almost same value of about 7.5° latitudes per 12 hours (about 55 km/hr) for all subregions except over ocean to the south of Japanese islands where the speed is a little slower.

As summarized above, the estimation of rainfall obtained from the IR imagery data of GMS has revealed some important aspects of the rainfall of the Baiu front, although it still has some deficiencies in accurancy and resolution. The further efforts toward approvement and extension of such a satellite-based rainfall estimation method are needed to supply more reliable data in global scale.

Acknowledgements

The author would like to thank Prof. Y. Mitsuta of the Disaster Prevention Research Institute (DPRI) of Kyoto University for his continous guidances and encouragements during the study. The author is also grateful to Dr. P. A. Arkin and Dr. J. E. Janowiak of NMC/NOAA, for supplying the satellite and ground data of AIP/1. Discussions with Prof. M. Yamada and other members in the Severe Storm Division of DPRI were very helpful. The computations were performed by FACOM M-730 computer at the Information Processing Center of DPRI.

References

1) Yoshino, M.M.: Four stages of rainy season in early summer over east Asia, Part 2. J.Met.Soc.Japan., Vol.44, 1966, pp.209-217.

2) Ninomiya, K., and T.Akiyama: Medium-scale echo clusters in the Baiu front as revealed by multi-radar composite echo maps. (Part 1) J.Met.Soc. Japan, Vol.50, 1972, pp.558-569.

3) Ninomiya, K., and T.Akiyama: Medium-scale echo clusters in the Baiu front as revealed by multi-radar composite echo maps. (part 2) J.Met.Soc. Japan, Vol.51, 1973, pp.108-118.

4) Akiyama, T.: The large-scale aspects of the characteristic features of the Baiu front. Pap.Met.Geophy., Vol.24, 1973, pp.157-188.

5) Akiyama, T.: Mesoscale pulsation of convective rain in medium-scale disturbancee developed in Baiu front. J.Met.Soc.Japan, Vol.56, 1978, pp.267-283.

6) Ninomiya, K., and H.Muraki: Large-scale circulations over East Asia during Baiu period of 1979. J.Met.Soc.Japan, Vol.64, 1986, pp.409-429.

7) Ninomiya, K., and H.Mizuno: Variations of Baiu precipitation over Japan in 1951-1980 and large-scale characteristics od wet and dry Baiu. J.Met. Soc.Japan, Vol.67, 1989, pp.639-658.

8) Akiyama, T.: Large, synoptic and meso scale variations of the Baiu front, during July 1982. Part 1: Cloud features. J.Met.Soc.Japan, Vol.67, 1989, pp.57-81.

9) Akiyama, T.: Large, synoptic and meso scale variations of the Baiu front, during July 1982. Part 2: Frontal structure and disturbances. J.Met. Soc.Japan, Vol.68, 1990, pp.557-574.

10) Akiyama, T.: Large, synoptic and meso scale variations of the Baiu front,

during July 1982. Part 3: Space-time scale and structure of frontal disturbances. J.Met.Soc.Japan, Vol.68, 1990, pp.705-727.

11) Arkin, P.A.: The relationship between fractional coverage of high cloud and rainfall accumulations during GATE over the B-scale array. Mon.Wea. Rev., Vol.107, 1979, pp.1382-1387.

12) Arkin, P.A. and B.N. Meisner: The relationship between large-scale convective rainfall and cloud cover over the western hemisphere during 1982-84. Mon.Wea.Rev., Vol.115, 1987, pp.51-74.

13) Shin, K-S., G.R.North, Y-S.Ahn and P.A.Arkin: Time scales and temporal variability of tropical oceanic rainfall. Mon.Wea.Rev., Vol.118,1990, pp.1507-1516.

14) Janowiak, J.E. and P.A.Arkin: Rainfall variations in the tropics during 1986-1989. J.Geophys.Res., Vol.96, 1991, pp.3359-3373.

15) Wylie, D.P.: An application of a geostationary satellite rain estimation technique to an extratropical area. J.Appl.Meteor., Vol.18, 1979, pp. 1640-1648.

16) Xie, P. and Y. Mitsuta: Rainfall estimation from GMS infrared and visible imagery data. Annuals. Disas. Prev. Res. Inst., Kyoto Univ., Vol.31B-1, 1988, pp.201-217. (in Japanese)

17) Xie, P.: Nephanalysis of the GMS imagery data. Bull. Disas. Prev. Res. Inst., Kyoto Univ., Vol.40, 1990, pp.57-77.

18) Xie, P.: Rainfall estimation in the midlatitudes from GMS infrared imagery data. Bull. Disas. Prev. Res. Inst., Kyoto Univ., Vol.41, 1991, pp.109-120.

19) Xie, P.: Estimation of rainfall on the Japanese islands and their adjacent ocean from satellite (GMS) infrared imgery. (submitted to Bull. Disas. Prev. Res. Inst., Kyoto Univ.)

20) Browning, K.A.: Rain, rainclouds and climate. Q.J.R.Meteorol.Soc., Vol.116, 1990, pp.1025-1051.

Captions

Fig. 1 The Baiu rainfall distribution for the period from June 24 to July 31, 1954. (After Yoshino[1])

Fig. 2 Spatial distributions of a) monthly averaged cloud amount and b) monthly accumulated rainfall of June 1989 over the investigation area.

Fig. 3 a) latitudinal and b) longitudinal profiles of rainfall (solid line) and cloud amount (dash line) over the investigation area.

Fig. 4 9 sub-regions in the area for investigating the rainfall features in various areas over both land and ocean. The latitudinal bound lines are at 41.25°N and 31.25°N. The longitudinal bound lines are at 122.5°E, 130.0°E and 141.25°E, respectively.

Fig. 5 Latitudinal distributions of daily rainfall (solid line) and daily-averaged cloud amount (dash line) relative to the position of surface front in the subregions. The results for the very north 3 subregions are not shown in the figture because no front moved in to the extent during the period. The surface front positions are read from the surface weather chart on 0900JST.

Fig. 6 Normalized spetral density (NSD) distributions of the time series of rainfall for the 9 subregions.

Fig. 7 Normalized spectral density (NSD) distribution of the time series of

rainfall averaged over all of the 9 subregions.

Fig. 8 Space-time Lagged correlations of the rainfall for all of the subregions except the very north three. The 5 lines in each figture show the correlations with time lags of -12, -6, 0, 6 and 12 hours, respectively. The value in the abscissa represents the longitudinal distance to the east of the reference point.

Table 1 Peak values of cloud amount and rainfall at Baiu front

A r e a	122.5-130.0E	130.0-141.25E	141.25-147.5E	122.5-147.5E
41.25-41.25N	0.72 94% 13.9 95%	0.85 111% 21.3 146%	0.85 111% 19.8 137%	0.81 107% 19.3 132%
22.50-31.25N	0.71 93% 11.0 75%	0.79 104% 14.0 96%	0.73 96% 14.0 96%	0.75 98% 12.3 84%
22.50-41.25N	0.71 93% 11.1 76%	0.80 105% 16.8 115%	0.77 101% 14.9 102%	0.76 100% 14.6 100%

Upper: cloud amount
Bottom: rainfall in mm

Table 2 Phase speeds of the movement
of rainfall region over various subregions

A r e a	122.5-130.0E	130.0-141.25E	141.25-147.5E	122.5-147.5E
41.25-41.25N	7.5	7.5	7.5	7.5
22.50-31.25N	7.5	5.0	7.5	6.25
22.50-41.25N	7.5	5.0	7.5	6.25

unit: °E/12hr

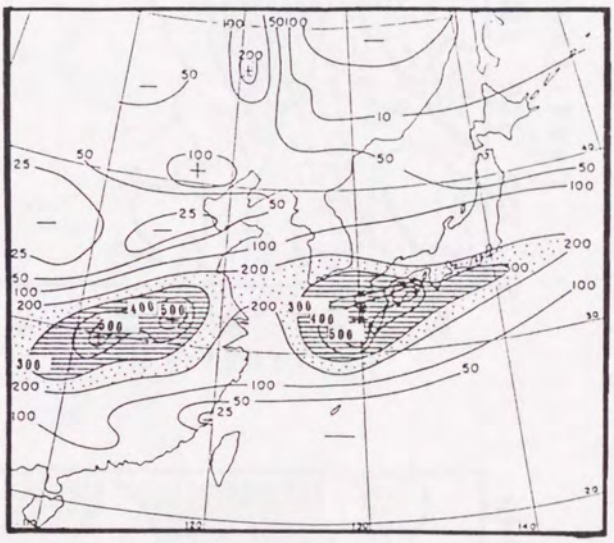
100
50
100
200
50
10
50
25
100
50
50
100
25
50
25
100
200
50
100
200
200
300
400
500
200
300
400
500
300
200
100
50
100
25
50
100
200
100
100
50
39
39
120
140

Fig. 1

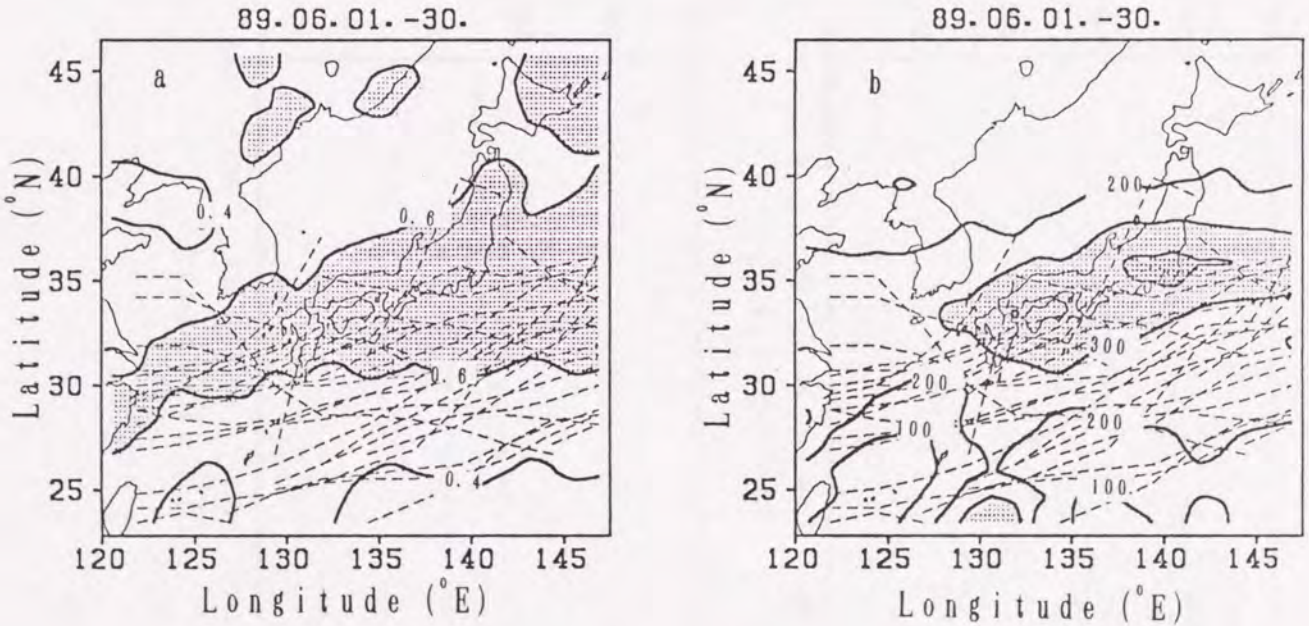
89. 06. 01. -30.
a
0. 4
0. 6
0. 6
0. 4
45
40
35
30
25
Latitude (°N)
120
125
130
135
140
145
Longitude (°E)
89. 06. 01. -30.
b
200
300
200
100
200
100
45
40
35
30
25
Latitude (°N)
120
125
130
135
140
145
Longitude (°E)

Fig. 2

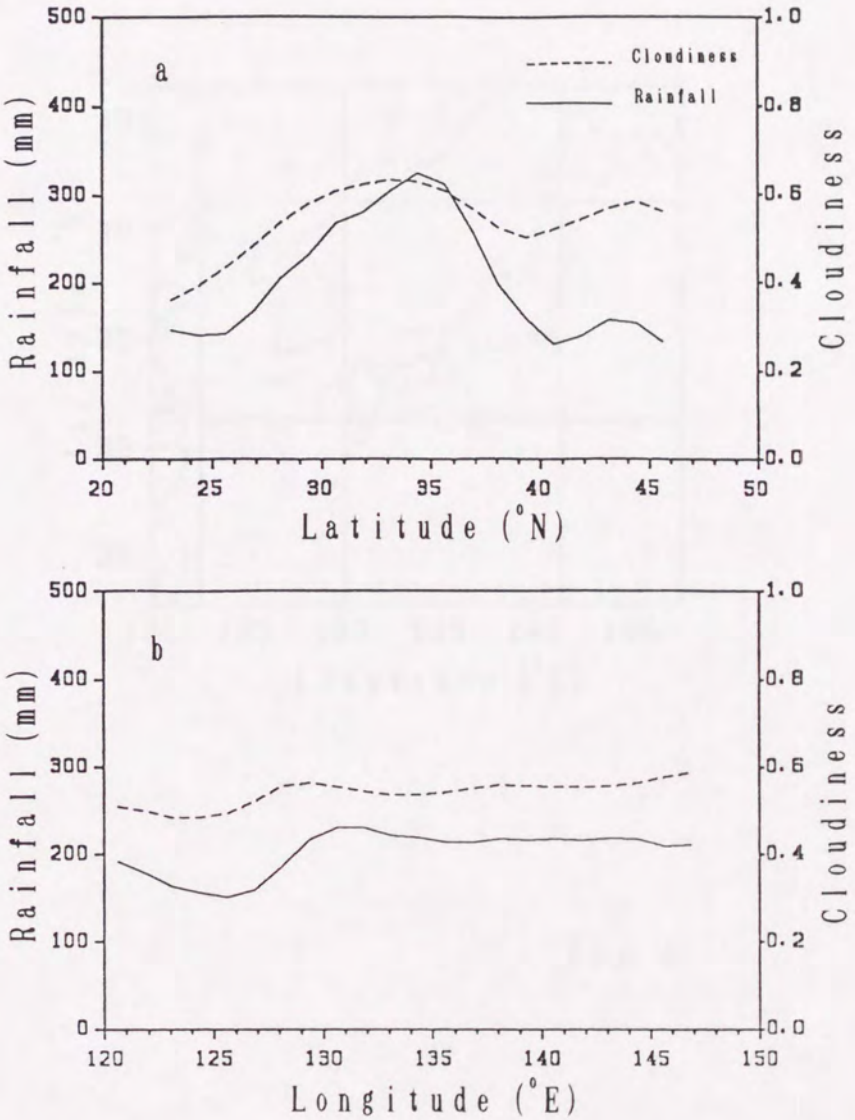
a
Cloudiness
Rainfall
Rainfall (mm)
Cloudiness
Latitude (°N)
b
Rainfall (mm)
Cloudiness
Longitude (°E)

Fig. 3

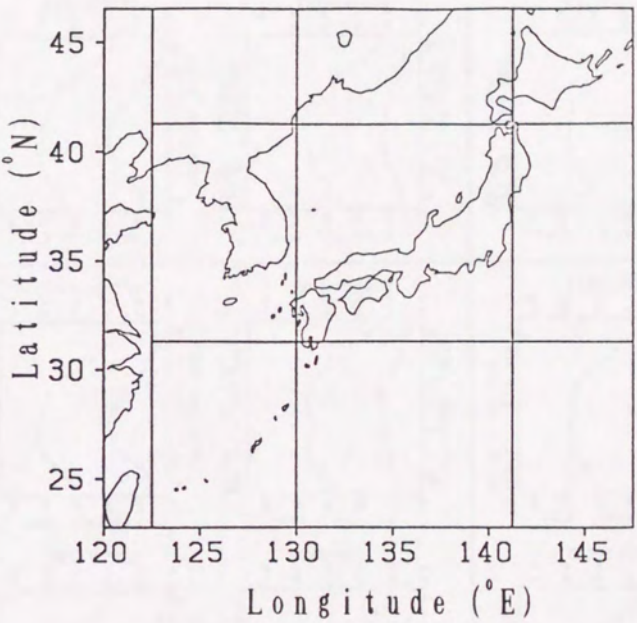

Fig. 4

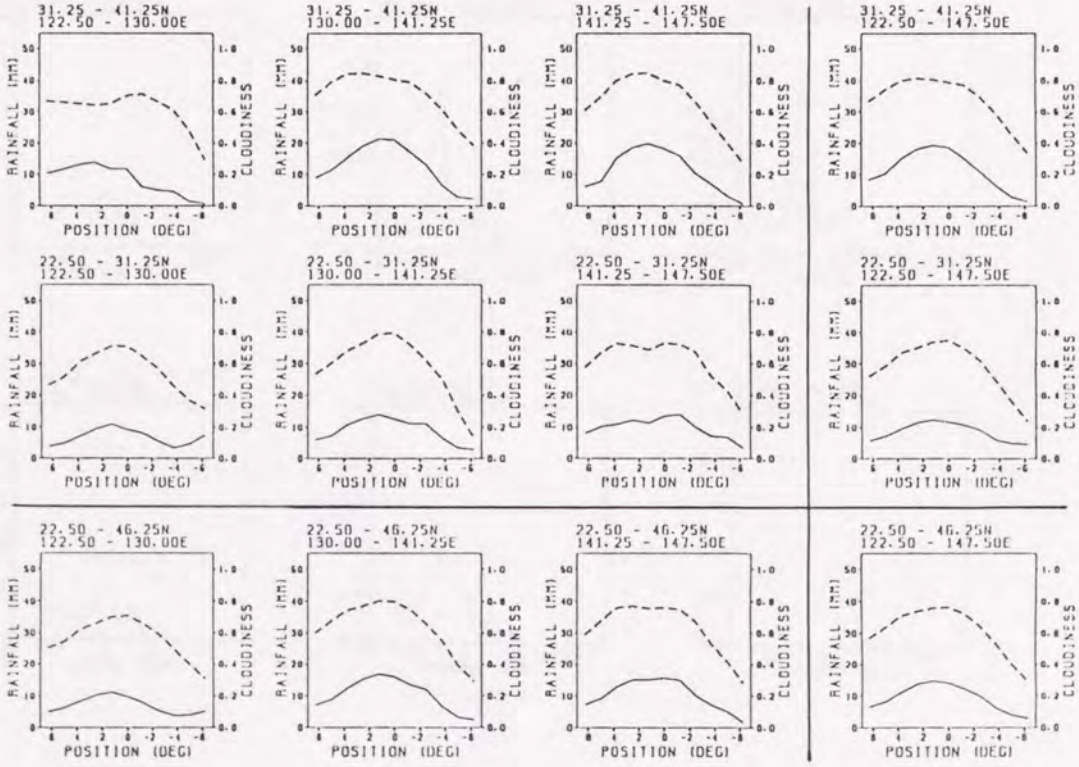
31.25 - 41.25N
122.50 - 130.00E
31.25 - 41.25N
130.00 - 141.25E
31.25 - 41.25N
141.25 - 147.50E
31.25 - 41.25N
122.50 - 147.50E
22.50 - 31.25N
122.50 - 130.00E
22.50 - 31.25N
130.00 - 141.25E
22.50 - 31.25N
141.25 - 147.50E
22.50 - 31.25N
122.50 - 147.50E
22.50 - 46.25N
122.50 - 130.00E
22.50 - 46.25N
130.00 - 141.25E
22.50 - 46.25N
141.25 - 147.50E
22.50 - 46.25N
122.50 - 147.50E
RAINFALL (MM)
CLOUDINESS
POSITION (DEG)

Fig. 5

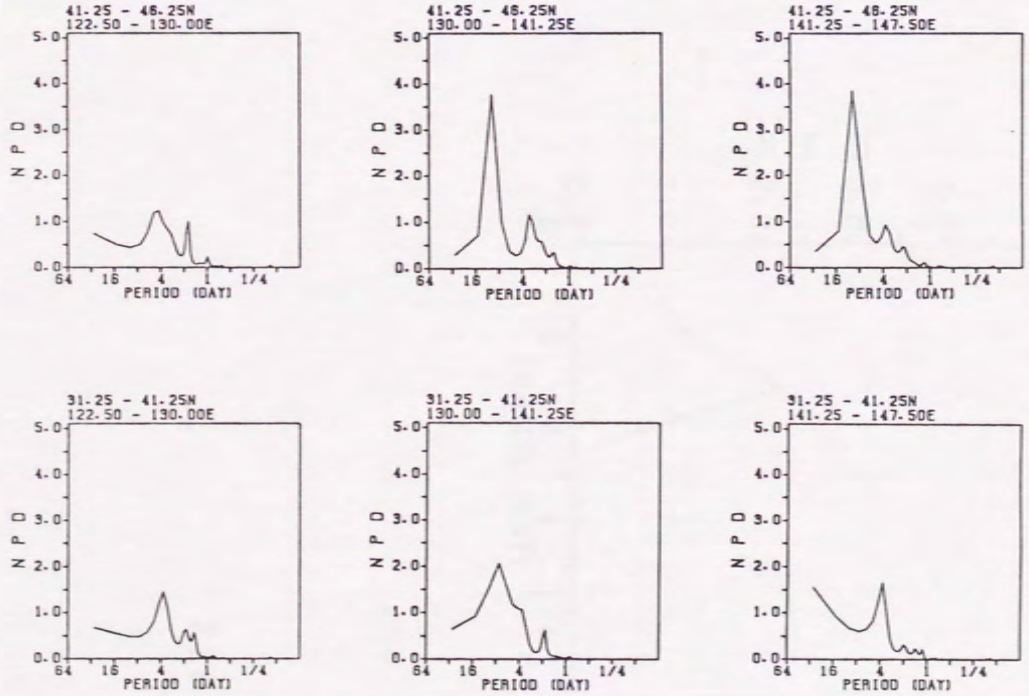
41.25 - 48.25N
122.50 - 130.00E
41.25 - 48.25N
130.00 - 141.25E
41.25 - 48.25N
141.25 - 147.50E
31.25 - 41.25N
122.50 - 130.00E
31.25 - 41.25N
130.00 - 141.25E
31.25 - 41.25N
141.25 - 147.50E
NPD
PERIOD (DAY)
64
16
4
1
1/4
0.0
1.0
2.0
3.0
4.0
5.0

Fig. 6

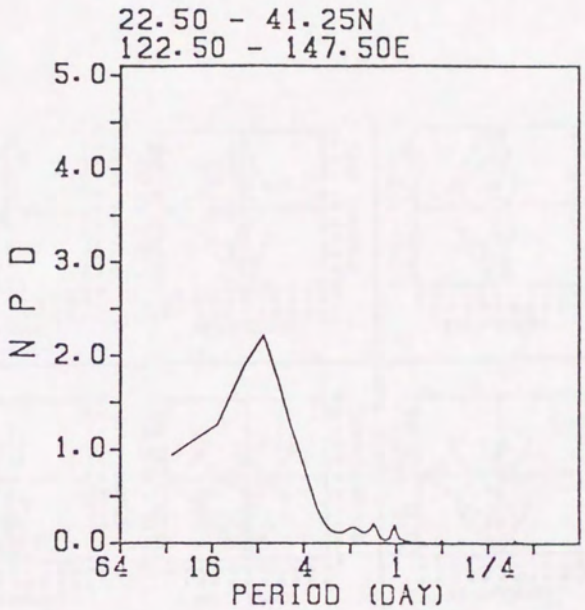
22.50 - 41.25N
122.50 - 147.50E
5.0
4.0
3.0
2.0
1.0
0.0
NPD
64
16
4
1
1/4
PERIOD (DAY)

Fig. 7

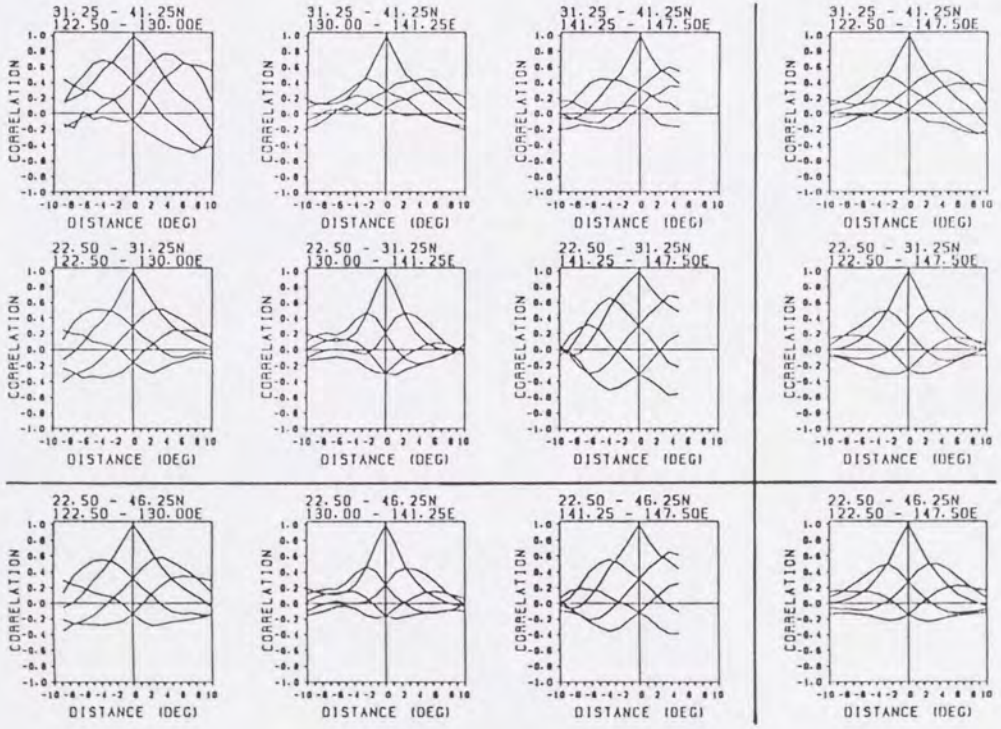
31.25 - 41.25N
122.50 - 130.00E
31.25 - 41.25N
130.00 - 141.25E
31.25 - 41.25N
141.25 - 147.50E
31.25 - 41.25N
122.50 - 147.50E
22.50 - 31.25N
122.50 - 130.00E
22.50 - 31.25N
130.00 - 141.25E
22.50 - 31.25N
141.25 - 147.50E
22.50 - 31.25N
122.50 - 147.50E
22.50 - 46.25N
122.50 - 130.00E
22.50 - 46.25N
130.00 - 141.25E
22.50 - 46.25N
141.25 - 147.50E
22.50 - 46.25N
122.50 - 147.50E
CORRELATION
DISTANCE (DEG)

Fig. 8